

Research Center for Molecular-Scale Nanoscience

IX-C Nano-science and Nano-Technology toward Molecular Scale Electronics

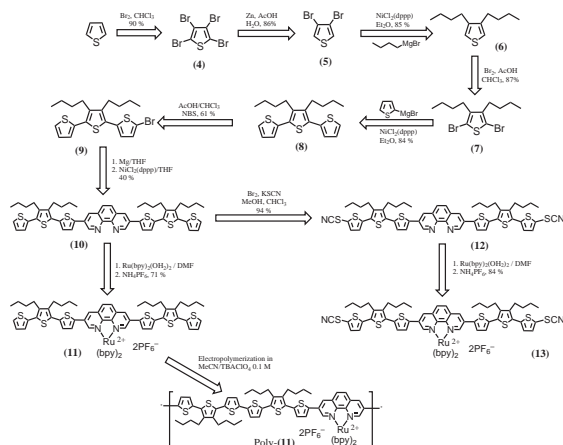
Studies on electric properties of organic and in-organic nano structures are challenging field in material science. Those of aggregates, crystals, or polymers which are made from a large number of molecules or atoms have been already established. In contrast, electronics of nano scale materials which are constructed from small number or single molecules are the forefront of science and technology, and have been revealed gradually to show their diverse phenomena such as quantum conductance, the Kondo effect, the Coulomb blockade, and resonance tunneling. In order to promote this field further, we are studying preparation or fabrication of new organic and in-organic nano materials, and developing new methods to measure their physical properties.

IX-C-1 Bridging Nano-Gap Electrodes by *In Situ* Electropolymerization of a Bis-Terthiophenylphenanthroline Ruthenium Complex

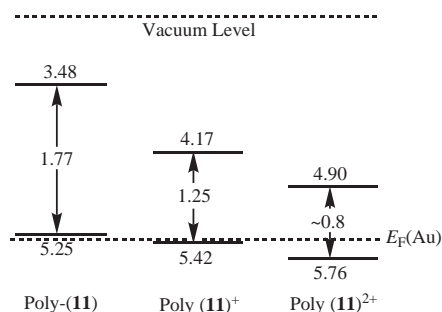
ARAKI, Koiti^{1,3}; ENDO, Hiroaki^{1,2}; MASUDA, Gou²; OGAWA, Takuji¹
(¹IMS, JST; ³Ehime Univ.; ³Univ. São Paulo)

[*Chem. Eur. J.* **10**, 3331–3340 (2004)]

A novel 3,8-bis-terthiophenyl-(1,10-phenanthroline) coordinated to [Ru(bpy)₂] was synthesized and characterized by electrochemical and spectroscopic techniques, and shown to be a suitable starting material for the electrodeposition of functionalized molecular wires in between nano-gap electrodes, generating stable molecular nano-devices. Temperature dependent non-linear *I-V* curves were obtained in the 80 to 300 K range. The material can be deposited on ITO also, forming compact electrochromic films at surface concentrations lower than about 1×10^{-8} mol·cm², but a more loosely bond fibrous form is preferentially deposited at higher surface concentrations.



Scheme 1.



Scheme 2.

IX-C-2 Multi Curve Fitting Analysis of Temperature Dependent *I-V* Curves of Poly-Hexathiophenephenanthroline Bridged Nano-Gap Electrodes

ARAKI, Koiti^{1,3}; ENDO, Hiroaki^{1,2}; TANAKA, Hirofumi¹; OGAWA, Takuji¹
(¹IMS, JST; ²Ehime Univ.; ³Univ. São Paulo)

[*Jpn. J. Appl. Phys.* **43**, L634–L636 (2004)]

Stable junctions were obtained by preparing poly-hexathiophenylphenanthroline coordinated wires to [Ru(bpy)₂] complexes directly in the Au electrode nano-gaps by electropolymerization. Reproducible non-linear and strongly temperature dependent curves, similar to that found for π -conjugated dithiols and diisocyanides self-assembled inside nano-holes, were obtained rather than a tunneling behavior commonly found in alkanethiol self-assembled monolayers. This is the first time that such a consistent series of data are collected for a polymer and interpreted based on a multi curve fitting method using a linear combination of tunneling, Frankel-Pool and hopping mechanism, suggesting that various independent conduction pathways may be present.

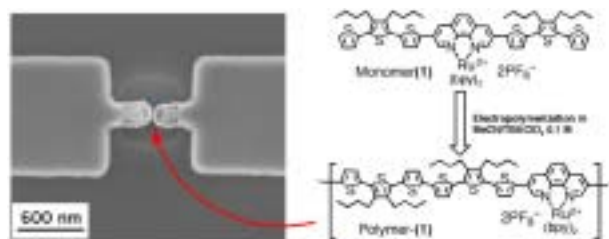


Figure 1.

IX-C-3 Position-Selected Molecular Ruler

TANAKA, Hirofumi; ANDERSON, Mary E.¹;
HORN, Mark W.¹; WEISS, Paul S.¹
(¹Pennsylvania State Univ.)

[*Jpn. J. Appl. Phys.* **43**, L950–L953 (2004)]

The molecular ruler method allows the precise control of the gap between a parent gold structure and a deposited daughter structure using a conveniently grown self-assembled molecular multilayer as a lithographic mask. However, we cannot choose a position where the gap should be placed, since the ruler attaches to all exposed gold surfaces. In this work, a convenient method of selecting the position of nano-gaps by further patterning the molecular multilayer using low-energy electron beam irradiation and piranha etchant is described.

The development of a convenient technique to fabricate precise nanostructures in large quantity is required for many types of application, such as electric devices, micromachines and biological equipment, since the “top-down” approach like electron lithography will reach its physical limit soon. Accordingly, it is urgently required to develop “bottom-up” techniques such as molecular self-assembly in order to achieve this goal.

Recently, many researchers have tried to create nano-gaps between electrodes to measure the electronic property of a single molecule or several molecules. For example, shadow evaporation, the break junction method and e-beam lithography have been investigated for this purpose. One of the most convenient approaches coupling the top-down and bottom-up approaches was developed as the molecular ruler method. This is based on the use of compact self-assembled molecular multilayers grown on a parent gold structure as a convenient photoresist. Gap width is precisely controlled by the length of the molecular ruler and the number of monolayers deposited on the top of parent structures, for example, prepared by conventional lithography techniques. One of the advantages of this method is that both sides of the gap are vertically parallel and the desired gap sides can be formed precisely. Another advantage is the position of the gap can be controlled. Multilayers are grown by the successive sequential deposition of monolayers of α,ω -mercaptoalkanoic acid ($\text{HS}(\text{CH}_2)_x\text{COOH}$) and Cu^{2+} ions, until desired thickness is achieved.

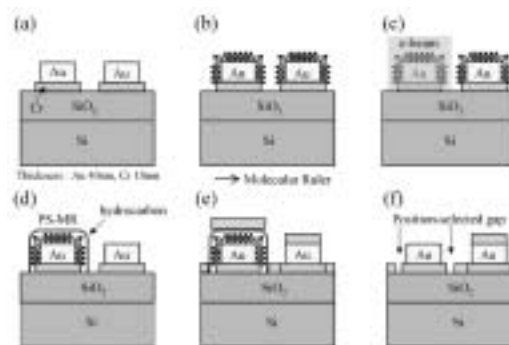


Figure 1.

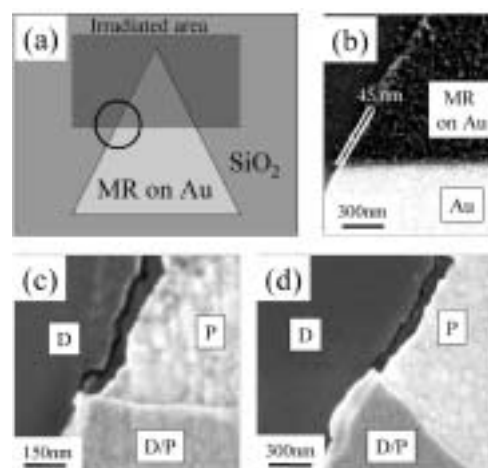


Figure 2.

IX-C-4 Advances in Nanolithography Using Molecular Rulers

ANDERSON, Mary E.¹; TAN, L. P.¹; TANAKA, Hirofumi²; MIHOK, M.¹; LEE, H.¹; HORN, Mark W.¹; WEISS, Paul S.¹
(¹Pennsylvania State Univ.; ²IMS and Pennsylvania State Univ.)

[*J. Vac. Sci. Technol. B* **21**, 3116–3119 (2003)]

The combination of conventional lithographic techniques with chemical self-assembly allows for the creation of nanostructures whose spacing and edge resolution reach nanometer-scale precision. The controlled placement and thickness of self-assembled multilayers composed of alternating layers of α,ω -mercaptoalkanoic acids and coordinated metal ions form precise molecular ruler resists that enable the production of tailored and lithographically defined metal patterns. Initial structures created by conventional techniques are referred to as parents and subsequent structures generated by the molecular ruler process are identified as daughters. We report the further creation of subsequent generation structures ~granddaughters! that have sub-100 nm dimensions. The granddaughter structures are created by forming molecular rulers on parent and daughter structures, and can be isolated by removing sacrificial parent and/or daughter structures. This process has also been utilized in combination with parent structures created by the process of nanosphere lithography to produce arrays

of metal features with 10 nm spacings. Since our original report, we have improved the throughput and reproducibility of the molecular ruler process by automating its iterative nature and by utilizing appropriate chemical lift-off solutions.

IX-C-5 Reactive Ligand-Protected Nano-Particles

**ARAKI, Koiti^{1,3}; MIZUGUCHI, Eisuke^{1,2};
TANAKA, Hirofumi¹; OGAWA, Takuji¹**
(¹IMS, JST; ²Ehime Univ.; ³Univ. São Paulo)

Gold nano-particles exhibit interesting bonding and electronic properties and have been proposed for many applications such as in photoelectrochemical devices, drug delivery systems and sensors. Such applications exploit the molecule-like electronic properties and the particle like behavior of such materials, behaving as highly dispersed solids possessing an exceedingly high functionalizable surface area. In fact, a very significant number of atoms constituting small nano-particles are in the surface and can bond species containing coordinating groups such as thiols, disulphides, phosphines, amines, *etc.* This means that almost any molecular species can be anchored in the surface imparting their physico-chemical properties to them or leading to the appearance of new properties. On the other hand electronic properties such as light absorption, excited state and electron-transfer characteristics can be controlled by changing the size and the nature of the surface anchored species.

As pointed out above, the preparation of nano-particles with narrow size distribution is a very important issue and some methods have been developed. For example, Brust *et al.* developed a general method for the preparation of thiol-protected gold-nanoparticles with a narrow size distribution, based on the reduction of AuCl_4^- in toluene with an aqueous NaBH_4 solution. The toluene solution also contains protecting species such as *n*-dodecanethiol, essential for the stabilization of the metal clusters, and tetraoctylammonium bromide (phase transfer agent). Teranishi *et al.* have shown that *n*-dodecanethiol protected Au-nanoparticles with very narrow size distribution can be obtained by controlled thermal treatment of previously prepared solid samples.

Another main issue for the widespread use of gold-nanoparticles is the sluggishness of the functionalization reactions, which in the case of *n*-dodecanethiol protected material generally can take more than a couple of days. To overcome such drawback more weakly binding protecting groups such as triphenylphosphine, amines and *tert*-dodecanethiol have been proposed. However, in the first case only very small (~1–2 nm diameter) nanoparticles can be obtained and the reactivity are not so much higher in any case. For this reason, even very unstable gold-nanoparticle solutions, obtained in the absence of coordinating organic protecting groups, have been employed. This starting material is quite unstable and should be used soon after its preparation, making almost impossible its proper characterization before use. This is a main issue since can compromise their applications. We disclosed a method for the preparation of highly reactive ligand-protected nanoparticles.

IX-D Development of Organic Semiconductors for Molecular Thin-Film Devices

Organic light-emitting diodes (OLEDs) and organic field-effect transistors (OFETs) based on π -conjugated oligomers have been extensively studied as molecular thin-film devices. Organic semiconductors with low injection barriers and high mobilities are required for highly efficient OLEDs and OFETs. Radical cations or anions of an organic semiconductor have to be generated easily at the interface with an electrode (or a dielectric), and holes or electrons must move fast in the semiconducting layer. Compared with organic *p*-type semiconductors, organic *n*-type semiconductors for practical use are few and rather difficult to develop. Recently, we found that perfluorinated oligomers are efficient electron-transport materials for OLEDs.

IX-D-1 Organic Thin-Film Transistors Based on Anthracene Oligomers

INOUE, Youji¹; TOKITO, Shizuo¹; ITO, Kaname;
SUZUKI, Toshiyasu

(¹NHK Sci. Tech. Res. Labs.)

[*J. Appl. Phys.* **95**, 5795–5799 (2004)]

OFETs with an active layer based on the organic semiconducting anthracene oligomers, 2,2'-bianthracene (**2A**), 2,6-trianthracene (**3A**), and their dihexyl derivatives (**DH-2A** and **DH-3A**), were fabricated. It was found that thin films of anthracene oligomers deposited by thermal evaporation had lamellar structures with a high degree of molecular ordering. Consequently, the OFETs based on anthracene oligomers showed high field-effect mobilities. The mobility of the OFETs was increased by the oligomerization and the substitution of alkyl groups. **DH-2A** on a SiO₂/Si substrate showed the highest mobility of 0.13 cm²/V s. It was also found that the electrical characteristics of the OFETs were improved by using a Ta₂O₅ gate insulator.

IX-D-2 Perfluoropentacene: High-Performance *p-n* Junctions and Complementary Circuits with Pentacene

SAKAMOTO, Youichi; SUZUKI, Toshiyasu;
KOBAYASHI, Masafumi¹; GAO, Yuan¹; FUKAI,
Yasushi¹; INOUE, Youji²; SATO, Fumio²;
TOKITO, Shizuo²

(¹Kanto Denka Kogyo; ²NHK Sci. Tech. Res. Labs.)

[*J. Am. Chem. Soc.* **126**, 8138–8140 (2004)]

We report the synthesis and characterization of perfluoropentacene as an *n*-type semiconductor for OFETs. Perfluoropentacene is a planar and crystalline material that adopts a herringbone structure as observed for pentacene. OFETs with perfluoropentacene were constructed using top-contact geometry, and the electron mobility of 0.11 cm²/V s was observed. Bipolar OFETs with perfluoropentacene and pentacene function at both negative and positive gate voltages. The improved *p-n* junctions are probably because of the similar d-spacings of both acenes. Complementary inverter circuits were fabricated, and the transfer characteristics exhibit a sharp inversion of the output signal with a high voltage gain.

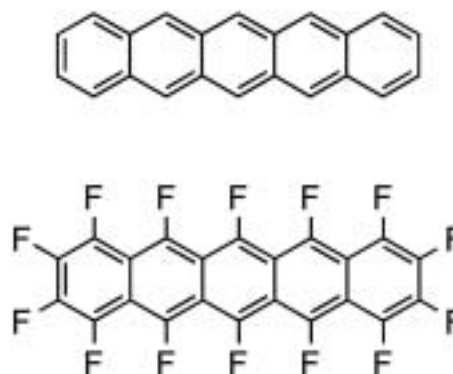


Figure 1. Structures of pentacene and perfluoropentacene.

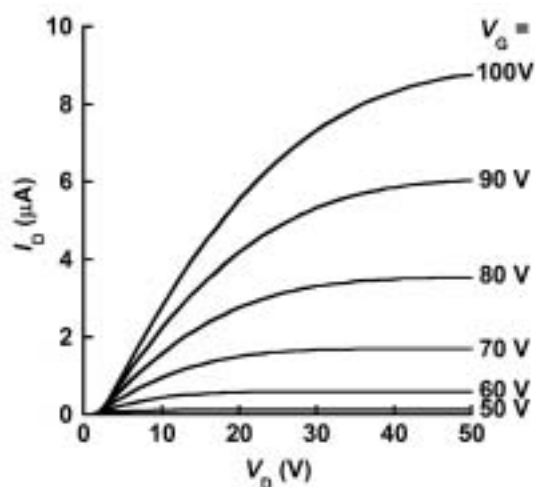


Figure 2. Drain current (I_D) versus drain voltage (V_D) characteristics as a function of gate voltage (V_G) for a perfluoropentacene OFET.

IX-E Field-Effect Transistors with Organic Semiconductors

Considerable attention has recently focused on organic field-effect transistors (OFET) because of their potential use in low-cost flexible electronic devices. We have studied output characteristics of OFET devices based on newly synthesized organic compounds.

IX-E-1 Field-Effect Transistors Based on Dicyanopyrazinoquinoxaline Derivatives

NISHIDA, Jun-ichi¹; NARASO¹; MURAI, Shiro¹; FUJIWARA, Eiichi; TADA, Hirokazu; TOMURA, Masaaki; YAMASHITA, Yoshiro¹
(¹Tokyo Inst. Tech.)

[*Org. Lett.* **6**, 2007–2010 (2004)]

Dicyanopyrazinoquinoxaline derivatives (Figure 1) have been prepared and characterized by using single-crystal X-ray structure analysis and redox potential measurements. They have strong electron-accepting properties due to the pyrazinopyrazine skeletons as well as the cyano groups. Substituents can be easily introduced at the benzene ring and control the HOMO-LUMO energy gap and the molecular packing. Figure 2 shows output characteristics of a bottom-contact OFET based on compound **1a**. It was found that the compound **1a** exhibited *n*-type semiconducting behavior with carrier mobility of $3.6 \times 10^{-6} \text{ cm}^2/\text{Vs}$. The compounds examined operated as *N*-type OFETs. The mobility and on/off ratio of the devices are summarized in Table 1.

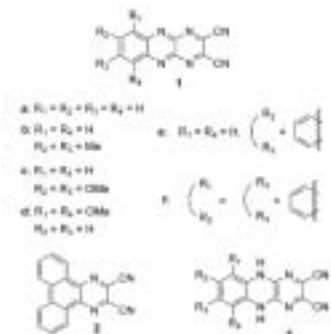


Figure 1. Molecular structures of dicyanopyrazinoquinoxaline derivatives.

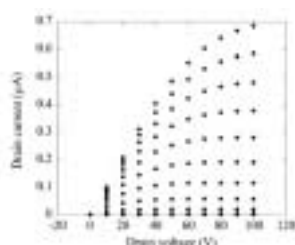


Figure 2. Output characteristics of the OFET based on compound **1a**. Gate voltages were varied from 0 to 100 V with an increment of 10 V.

Table 1. Field-effect mobilities and on/off current ratios of FETs based on dicyanopyrazinoquinoxaline derivatives.

	mobilities (cm ² /V·s)	on/off
1a	3.6×10^{-6}	10 ²
1b	1.8×10^{-4}	10 ³
1c	2.1×10^{-4}	10 ³
1d	2.5×10^{-4}	10 ³
1e	2.2×10^{-4}	10 ³
1f	5.5×10^{-4}	10 ³
2		

IX-E-2 Low-Voltage Organic Field-Effect Transistors Based on Ta₂O₅ as Gate Insulator Material

SAKAI, Heisuke¹; FURUKAWA, Yukio¹; FUJIWARA, Eiichi; TADA, Hirokazu
(¹Waseda Univ.)

[*Chem. Lett.* in press]

A thin film of Ta₂O₅ was prepared by sputtering on heavily-doped silicon substrates and used as a gate insulator of field-effect transistors. Poly(2-methoxy-5-(2'-ethylhexyloxy)-1,4-phenylenevinylene) (MEH-PPV) and pentacene were used as active semiconductors. Interdigital Au electrodes, which consisted of 25 pairs with 25 μm in spacing, 4 mm in width, and 50 nm in thickness, were prepared on the organic layer and used as the source and drain electrodes. Clear saturation in drain currents was observed at low drive voltage of about -3 V as shown in Figure 1. MEH-PPV and pentacene exhibited *p*-type semiconducting behaviors with mobilities of $4.6 \times 10^{-4} \text{ cm}^2/\text{V s}$ and $0.8 \text{ cm}^2/\text{V s}$, respectively.

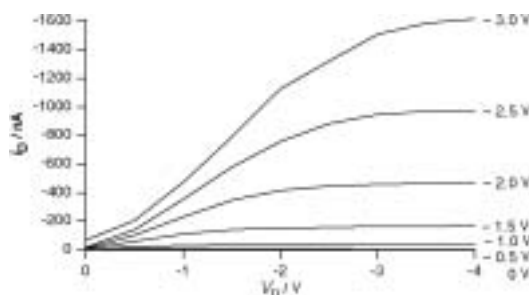


Figure 1. Output characteristics of an FET based on MEH-PPV with a Ta₂O₅ gate insulator.

IX-E-3 Visible Light Emission from Polymer-Based Field-Effect Transistors

SAKANOUE, Tomo¹; FUJIWARA, Eiichi; YAMADA, Ryo; TADA, Hirokazu
(¹GUAS)

[*Appl. Phys. Lett.* **84**, 3037–3039 (2004)]

Field-effect transistors (FETs) based on poly [2-methoxy, 5-(2'-ethyl-hexoxy)-1,4-phenylenevinylene] (MEH-PPV) were prepared with bottom-contact type interdigital electrodes of Cr/Au and Al/Au on the SiO₂/Si substrates. MEH-PPV exhibited a *p*-type semiconducting behavior and orange light emission was observed when the devices were operated in vacuum. It was found that the luminescence efficiency of the FETs with Al/Au electrodes was higher than that of Cr/Au electrodes, as shown in Figure 1. The simultaneous injection of holes and electrons into MEH-PPV occurred efficiently with the application of Al/Au heteroelectrodes.

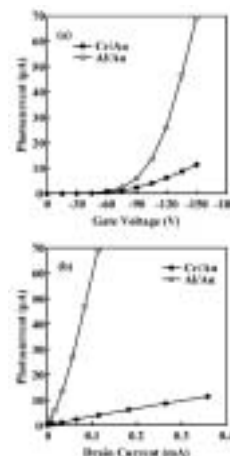


Figure 1. Luminescence intensity detected with a Si photodiode as a function of the gate voltage (a) and the drain current (b). The drain voltage was set at -150 V.

IX-F Molecular Assemblies on Silicon Surfaces via Silicon–Carbon Covalent Bonds

Preparation of molecular assemblies on inorganic semiconductors such as silicon and germanium has received a growing interest because of their potential application to stable regist for nano-patterning. We have prepared organic monolayers on silicon by wet process and studied film structures with IR and AFM.

IX-F-1 Temperature Dependence of the Structure of Alkyl Monolayers on Si(111) Surface via Si–C Bond by ATR-FT-IR Spectroscopy

YAMADA, Ryo; ARA, Masato¹; TADA, Hirokazu (¹GUAS)

[*Chem. Lett.* **33**, 492–493 (2004)]

The temperature dependence of C–H stretching modes of alkyl monolayer formed on Si(111) surface was investigated by an attenuated total reflection Fourier transform infrared spectroscopy from room temperature up to 540 K. Continuous disordering of the monolayer was indicated from the gradual peak shifts toward higher frequency in C–H stretch modes upon heating. The irreversible conformational disorder was introduced in the monolayer above 440 K.

IX-F-2 Non-Contact Atomic Force Microscopy Using Silicon Cantilevers Covered with Organic Monolayers via Silicon–Carbon Covalent Bonds

ARA, Masato¹; SASAHARA, Akira²; OHNISHI, Hiroshi²; TADA, Hirokazu (¹GUAS; ²KAST)

[*Nanotechnology* **15**, S65–S68 (2004)]

Silicon cantilevers covered with dodecyl monolayers anchored via silicon–carbon covalent bonds were prepared by a wet process and used for non-contact atomic force microscopy (NC-AFM) of TiO₂(110)–(1×1) surfaces. Figure 1 shows an AFM image of the surface taken with the dodecyl-coated cantilevers. Clear images of atomic rows on atomically flat terraces were observed when the substrate was biased around 2.0 V with respect to the cantilevers. The bias voltage required to give clear images for alkyl-coated cantilevers was higher than that for uncoated ones. Since the cantilevers are thermally and chemically stable, they are applicable to various force microscopy to distinguish chemical species on surfaces.



Figure 1. NC-AFM image of the TiO₂ surface (10 nm × 10 nm). The frequency shift and sample bias voltage were set at -186 Hz and 2 V, respectively.

IX-G Low Temperature Scanning Tunneling Microscopy and Spectroscopy of Organic Molecules on Metal Surfaces

The electronic structure of molecules adsorbed by metal surfaces is of growing interest in the field not only of surface science but also of molecular-scale electronic devices. Scanning tunneling microscopy and spectroscopy are powerful tool to investigate molecular arrangements and electronic structure with atomic resolution. We have prepared epitaxial films of phthalocyanine molecules on clean metal surfaces and studies there structures by scanning tunneling microscopy and spectroscopy at low temperature.

IX-G-1 Low Temperature Scanning Tunneling Microscopy of Phthalocyanine Multilayers on Au(111) Surfaces

TAKADA, Masaki¹; TADA, Hirokazu
(¹GUAS)

[*Chem. Phys. Lett.* **392**, 265–269 (2004)]

We have studied epitaxial trilayer films of cobalt-phthalocyanine (CoPc) on Au(111)- $22\times\sqrt{3}$ surfaces using a scanning tunneling microscope at 78 K. Figure 1 shows an STM image of a CoPc monolayer on the Au(111) surface. Molecules in each layer were found to form square lattices and stacked along the $[1\bar{1}0]$ axis of the Au(111) surface. While CoPc molecules in the first layer were observed at bias voltages of -2.5 to $+2.5$ V,

there were certain ranges of bias voltage in which molecules in the upper layers were invisible. The electronic structures of molecules in upper layers are more localized than those of the first layer, which is affected by the substrate surface.

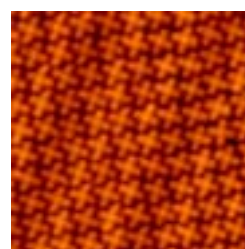


Figure 1. STM image of CoPc molecules on the Au(111) surface (14.6 nm \times 14.6 nm).

IX-H Development of New Transport Mechanism Based on Wetting Gradients

Construction and control of wetting gradients on surfaces are of growing interest since the spatiotemporal control of wetting leads to non-mechanical pumping systems in micro-fluidic devices. The imbalance of surface tensions is known to play an important role in the movement of droplets on surfaces. We have succeeded in the reversible control of the direction, magnitude and position of the wetting gradient by in-plane regulation of the electrochemical potential of the thin-film substrate covered with a redox-active self-assembled monolayer. A small droplet of organic liquid was shown to move under the cyclic shift of wetting gradient in aqueous solutions.

IX-H-1 Electrochemically Generated Wetting Gradient and Its Application for the Transport of Droplets

YAMADA, Ryo; TADA, Hirokazu

The in-plane voltage (V_{bias}) was applied to the gold thin film substrate covered with 11-Ferrocenyl-1-undecanethiol (FcC11SH) in addition to the conventional potentiostatic regulation of the potential of the substrate with respect to the reference electrode (RE) (Figure 1a). The current flowing through the substrate causes a continuous potential drop in it. The surface covered with FcC11SH monolayer is known to be hydrophobic and hydrophilic when Fc is reduced and oxidized, respectively. When the potential in the substrate crosses the oxidation potential of the FcC11SH monolayer, a gradient in the extent of oxidation of

the ferrocene, and thus, the wetting across the surface is generated (Figure 1b). The generation and regulation of wetting gradient by this method was confirmed by observing the shape of three droplets of nitrobenzene aligned in the biased direction. The one (Figure 2a; left was more negative) and two (Figure 2b) of the droplets got wet as the V_{bias} was increased. Since the electrochemical reaction of ferrocene is reversible, the observed wetting transition was reversible. Position of the wetting gradient can be moved by E_{offset} and direction and magnitude of it are controlled by V_{bias} in Figure 1a. The spatiotemporal control of the wetting gradient enabled us to manipulate a droplet on a substrate. Figure 3 shows the droplet moved in inchworm-like manner. Initially, the wetting gradient was positioned in the left of the picture and the left side of the substrate was wetting in Figure 3a. As wetting region reached the droplet, droplet spread into left, *i.e.*, wetting area as

shown in Figure 3b. When the position of the wetting gradient was reversed, the droplet shrunk from the right side in Figure 3c. As a result, a net transport of the droplet took place.

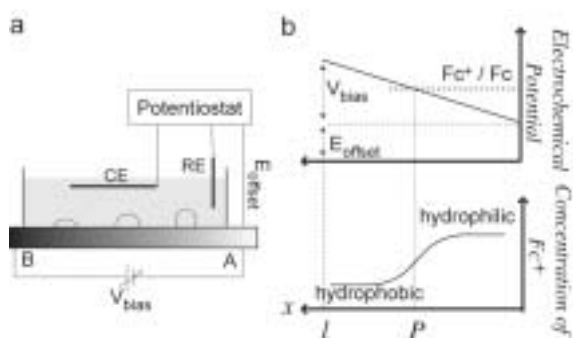


Figure 1. (a) Schematic drawing of the experimental configuration. (b) Potential profile and wetting distribution on the substrate under the biased condition.

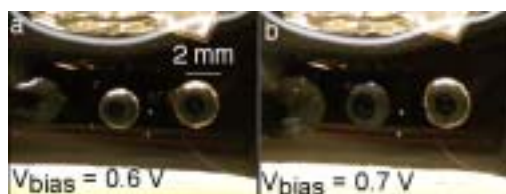


Figure 2. The formation of the wetting gradient by V_{bias} . V_{bias} was -0.6 V (a) and -0.7 V (b). E_{offset} was -300 mV vs. AuO_x .

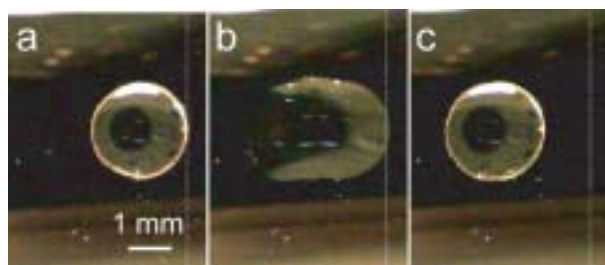


Figure 3. Inchworm motion of the droplet in the solution. See text for details. E_{offset} = (a) -300 mV, (b) -340 mV and (c) -300 mV.

IX-I Development of Precisely-Defined Macromolecules and Their Organization on Substrate Surfaces for Planar Molecular-Scale Electronics Circuits

The concept of molecular-scale electronics is now realized for individual components such as wire, diode, switch, and memory cell, but the fabrication of complete molecular-scale circuits remains challenging because of the difficulty of connecting molecular modules to one another. Molecular monolithic technology, which integrates the wiring, transistors and the required passive elements on a single macromolecule, has been proposed as a promising solution to this problem. In this project we have been trying to establish both the architecture of this novel class of macromolecules and the protocols for their purposive organization on metal/semiconductor substrate surfaces.

IX-I-1 Partially Insulated Molecular Wire as Components for Planar Molecule-Metal Junctions

TANAKA, Shoji

We have developed a series of “partially-insulated” multi-nanometer oligothiophenes to investigate systematically the nature of planar molecule-metal junctions as shown in Figure 1. Charge transport at planar junctions will be controlled by the degree of face-to-face interactions between π -system of conjugated molecules and electrode substrate. Therefore, to define exactly the areas of interactions, we have designed these molecules; the main chain consists of bare π -system as “charge-transfer interface” and insulated π -system possessing electron-donating amino groups as “positive charge-retention sites.” Here we describe the electrochemical characterization of these molecules.

Figure 2 shows the cyclic voltammograms of the partially insulated oligothiophenes and the related molecules. In general multi-scan voltammogram of long oligothiophenes ($> \alpha$ -6T) is well known to be ill defined as shown in the voltammogram of oligomer **1**. The complicated electrochemical behavior can be attributed to severe interchain interactions among the charged long oligomers that induce molecular aggregation and deposition on the electrode. During these processes, charges on an oligomer are dispersed and lost. In contrast, partially insulated oligothiophenes **3,4,6** as well as the fully insulated one **2** afforded reversible steady-state voltammograms. These findings suggest that only a one third coverage of the main chain of the α -9T-18T is enough to reduce the interchain interactions between the charged species and prevent the aggregation. In the case of oligomer **5**, slight voltammogram deformation, a symptom of aggregation, was observed. This indicates that the steric hindrance of the alkyl substituents on the interchain interactions is minor but not negligible.

Figure 3 shows the differential pulse voltammograms of partially insulated oligothiophenes **2-4**. Judging from the potential difference between the first and second peak, the magnitude of on-site Coulomb repulsion was found to decrease in this order: **4** $>$ **2** $>$ **3**. This result may be explained based on the spatial arrangement of the insulated mantle. This component has electron-donating amino groups and tends to attract positive charges. Therefore, separate

arrangement of them in the main chain is expected to isolate positive charges from each other resulting in reduction of on-site Coulomb repulsions as illustrated in Figure 3.

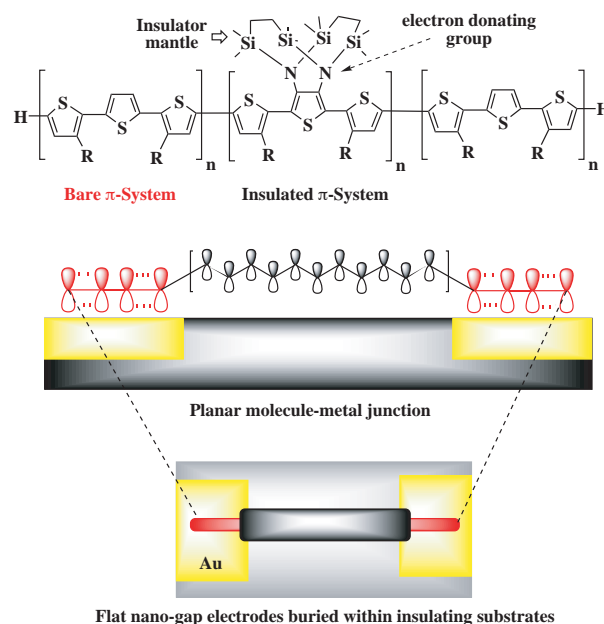


Figure 1. Molecular structure of partially insulated oligothiophenes.

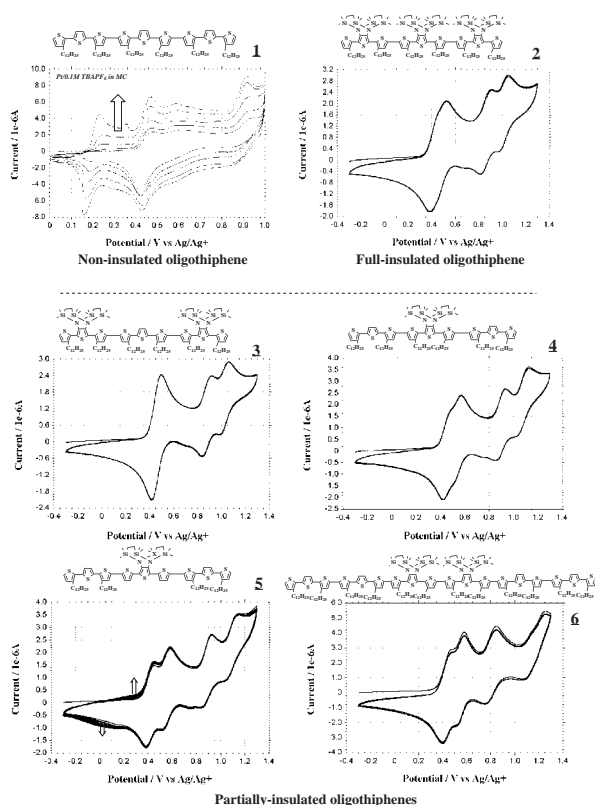


Figure 2. Cyclic voltammograms of oligothiophenes.

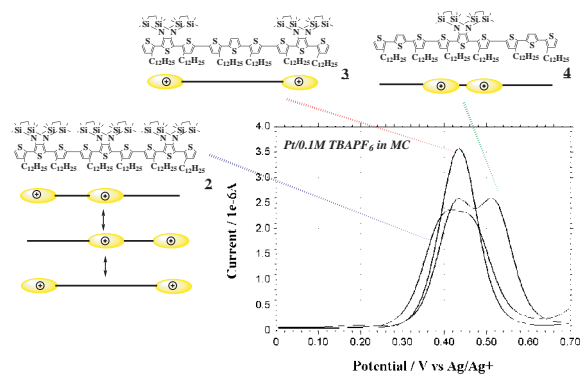


Figure 3. Differential pulse voltammograms of oligothiophenes.

IX-J Development of Novel Heterocyclic Compounds and Their Molecular Assemblies for Advanced Materials

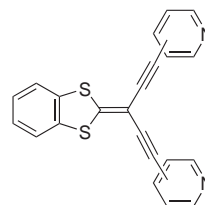
Heterocycles containing sulfur and/or nitrogen atoms are useful as components of functional materials since heteroatoms in their rings are helpful to stabilize ions or ion-radical species, and extended π -conjugation decreases Coulombic repulsion. In addition intermolecular interactions caused by heteroatom contacts can be expected to form novel molecular assemblies. In this project new electron acceptors, donors, and donor-acceptor compounds based on heterocycles such as 1,2,5-thiadiazole and 1,3-dithiole were synthesized and their properties including those of the charge-transfer complexes or ion-radical salts were investigated. Unique crystal structures were constructed by using weak intermolecular interactions such as hydrogen bonding or heteroatom contacts.

IX-J-1 Preparation, Structures and Properties of Novel 1,3-Dithiol-2-Ylidene Derivatives Containing Bis(ethynylpyridine) Units

KUMAGAI, Tsutomu¹; TOMURA, Masaaki;
NISHIDA, Jun-ichi¹; YAMASHITA, Yoshiro²
(¹Tokyo Inst. Tech.; ²IMS and Tokyo Inst. Tech.)

[*Tetrahedron Lett.* **44**, 6845–6848 (2003)]

1,3-Dithiol-2-ylidene derivatives containing bis(ethynylpyridine) units were synthesized using a Pd-catalyzed reaction of the corresponding dibromide. X-Ray crystal analysis revealed unique crystal structures depending on the aromatic groups. The absorption spectra and redox properties indicated intramolecular charge-transfer interactions between the 1,3-dithiole unit and the pyridyl parts.



2-dipyridyl, 3-dipyridyl, 4-dipyridyl

IX-J-2 (1,3-Dithiol-2-ylidene)propanedinitrile

TOMURA, Masaaki; YAMASHITA, Yoshiro¹
(¹IMS and Tokyo Inst. Tech.)

[*Acta Crystallogr., Sect. E* **59**, o1941–o1943 (2003)]

In the crystal structure of the title compound, C₆H₂

N_2S_2 , there is a tape structure, as a result of C–H...N hydrogen bonds is found. The molecules stack along the [120] direction in a head-to-tail fashion.

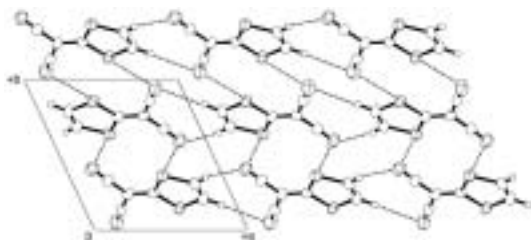


Figure 1. Packing diagram of the title compound viewed along the *c* axis. Dashed lines show the intermolecular S...N and C–H...N contacts.

IX-J-3 Crystal Structure of 4,7-Dibromo-2,1,3-Benzothiadiazole, $C_6H_2Br_2N_2S$

TOMURA, Masaaki; YAMASHITA, Yoshiro¹
(¹IMS and Tokyo Inst. Tech.)

[*Z. Kristallogr. NCS* **218**, 555–556 (2003)]

The title compound crystallizes in a centrosymmetric $P2_1/c$ space group with two crystallographically independent molecules in the asymmetric unit. The considerable shortenings of the C1–C6, C4–C5, C7–C12 and C10–C11 bonds are observed. Such double bond fixation suggests the quinonoid character of the 2,1,3-benzothiadiazole ring. Short S...N and Br...Br intermolecular heteroatom contacts are found in the crystal. The S...N [3.226(4) and 3.238(4) Å] and the Br...Br [3.542(1) and 3.662(1) Å] distances are 3.4–3.7% and 1.0–4.3% shorter than the sum of the corresponding van der Waals radii, respectively.

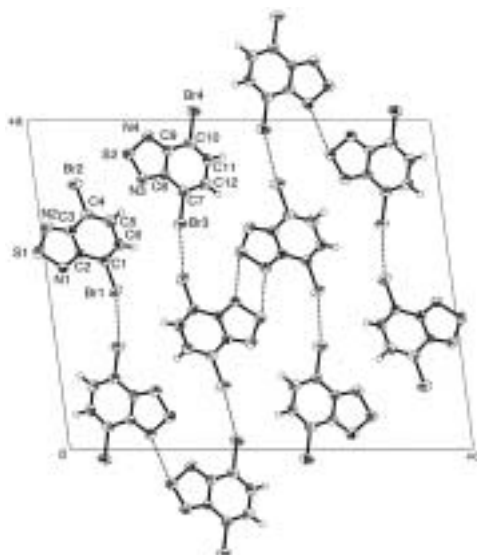


Figure 1. Packing diagram of the title compound viewed along the *b* axis. Dashed lines show the short intermolecular S...N and Br...Br contacts.

IX-J-4 4,5-Diiodo[1,2,5]thiadiazolotetrathiafulvalene

TOMURA, Masaaki; YAMASHITA, Yoshiro¹
(¹IMS and Tokyo Inst. Tech.)

[*Acta Crystallogr., Sect. E* **60**, o63–o65 (2004)]

In the crystal structure of the title compound, 5-(4,5-diiodo-1,3-dithiol-2-ylidene)-1,3-diaza-2,4,6-trithiapentalene, $C_6I_2N_2S_5$, a large number of short intermolecular heteroatom contacts, such as S...N, S...S, S...I, N...I, and I...I, are observed. The molecules, which are planar within 0.051 Å, stack along the *b* axis in a head-to-head fashion.

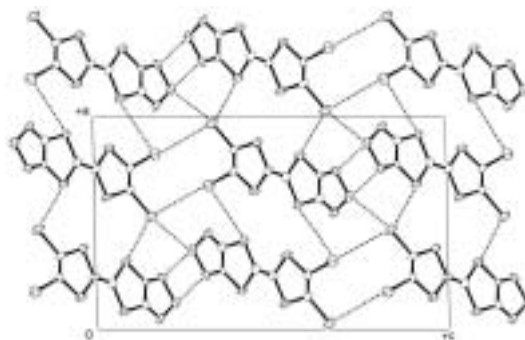


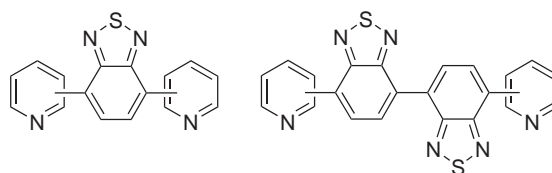
Figure 1. Packing diagram of the title compound viewed along the *b* axis. Dashed lines indicate the short intermolecular S...N, S...I and I...I contacts.

IX-J-5 Synthesis and Characterization of Novel Dipyridylbenzothiadiazole and Bisbenzothiadiazole Derivatives

AKHTARUZZAMAN, Md.¹; TOMURA, Masaaki;
NISHIDA, Jun-ichi¹; YAMASHITA, Yoshiro²
(¹Tokyo Inst. Tech.; ²IMS and Tokyo Inst. Tech.)

[*J. Org. Chem.* **69**, 2953–2958 (2004)]

Novel dipyridyl compounds containing a mono- and bisbenzothiadiazole unit were synthesized using the Stille coupling reaction. Their pyridinium salts, viologen analogues, were also prepared by the N-alkylation. The X-ray crystallographic analysis of the compounds containing a benzothiadiazole ring revealed nonplanar molecular structures and unique crystal structures depending on the nitrogen positions. The dipyridyl compounds are efficient fluorophores with high electron affinity. The derivative afforded complexes with chloranilic acid and cyanuric acid composed of hydrogen bonding networks. The methyl viologen analogues showed two-stage one-electron reduction waves.



2,2'-dipyridyl, 3,3'-dipyridyl, 4,4'-dipyridyl

IX-K Aquacatalysis

Catalytic organic transformations under mild, safe, and green conditions are important goals in synthetic organic chemistry. We recently reported that several palladium-catalyzed reactions, including π -allylic substitution, carbonylation, the Heck reaction, and Suzuki-Miyaura cross-coupling, took place in water by use of palladium-phosphine complexes bound to an amphiphilic polystyrene-poly(ethylene glycol) graft copolymer (PS-PEG) resin. Rhodium-catalyzed hydroformylation, cyclotrimerization of alkynes, and Michael-type addition of arylboronic acids were also found to proceed smoothly in water. Here we wish to report recent progress in this subject.

IX-K-1 Catalytic Oxidation of Alcohols in Water under Atmospheric Oxygen by Use of an Amphiphilic Resin-Dispersion of Nano-Palladium Catalyst

UOZUMI, Yasuhiro; NAKAO, Ryu

[*Angew. Chem., Int. Ed.* **42**, 194–197 (2003); *Angew. Chem.* **115**, 204–207 (2003)]

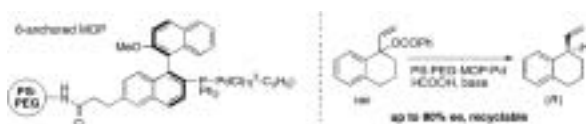
An amphiphilic polystyrene-poly(ethylene glycol) resin-dispersion of palladium nanoparticles was designed and prepared with a view toward use for catalysis in water. The catalytic aerobic oxidation of various alcohols forming aldehydes, ketones, and carboxylic acids was achieved in water under atmospheric pressure conditions by use of the PS-PEG supported nano-palladium catalyst.



IX-K-2 PS-PEG Resin-Supported Palladium-MOP Complexes. Application in Asymmetric π -Allylic Reduction

UOZUMI, Yasuhiro; HOCKE, Heiko

Homochiral palladium complexes of polymeric 2',-6-, and 6'-anchored 2-diphenylphosphino-1,1'-binaphthyl (MOP) ligands were prepared on polystyrene-poly(ethylene glycol) (PS-PEG) resin. The PS-PEG resin-supported palladium-MOP complexes exhibited high catalytic activity, stereoselectivity (up to 80% ee), and recyclability (6 times) in the asymmetric allylic reduction of 1-vinyl-1,2,3,4-tetrahydronaphth-1-yl benzoate to give 1-vinyl-1,2,3,4-tetrahydronaphthalene.



IX-L Development of New Nanomaterials as Components in Advanced Molecular Systems

Nanometer-sized materials exhibit unique electronic behavior. In the quest of advanced redox catalysis, we are currently interested in combining nanometer-sized materials into molecular redox systems. As a basic architecture, a new type of dendrimers were synthesized and their dynamic behavior was examined.

IX-L-1 Synthesis and Properties of New, Spatially Relaxed Dendrons Containing Internal Carboxyl Groups

KIKUZAWA, Yoshihiro; NAGATA, Toshi

[*Bull. Chem. Soc. Jpn.* **75**, 993–1000 (2004)]

We synthesized a series of new dendrons with up to fourteen internal carboxyl groups. These dendrons are made from a branching unit and a spacer unit with a carboxyl group. The growth reactions (formation of the benzylic ether bonds) completed within a few hours, which suggests the high reactivity at the “focal” point of the dendritic framework. The final deprotection of the internal ester groups also proceeded smoothly. These high reactivities were attributed to the presence of the spacer units, which caused spatially relaxed conformations of these molecules. The carboxylate salt form of the dendron produced both normal and reverse micelles in a THF/water mixed solvent according to the fraction.

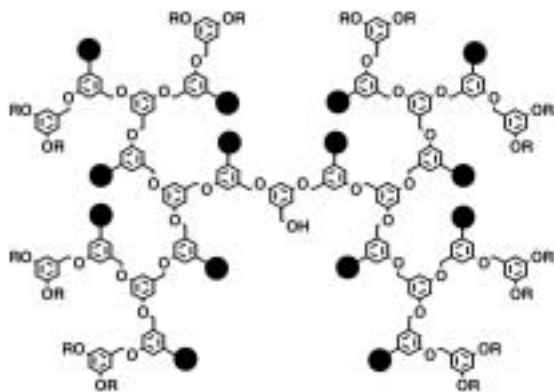


Figure 1. The chemical structure of the dendron (generation 3).

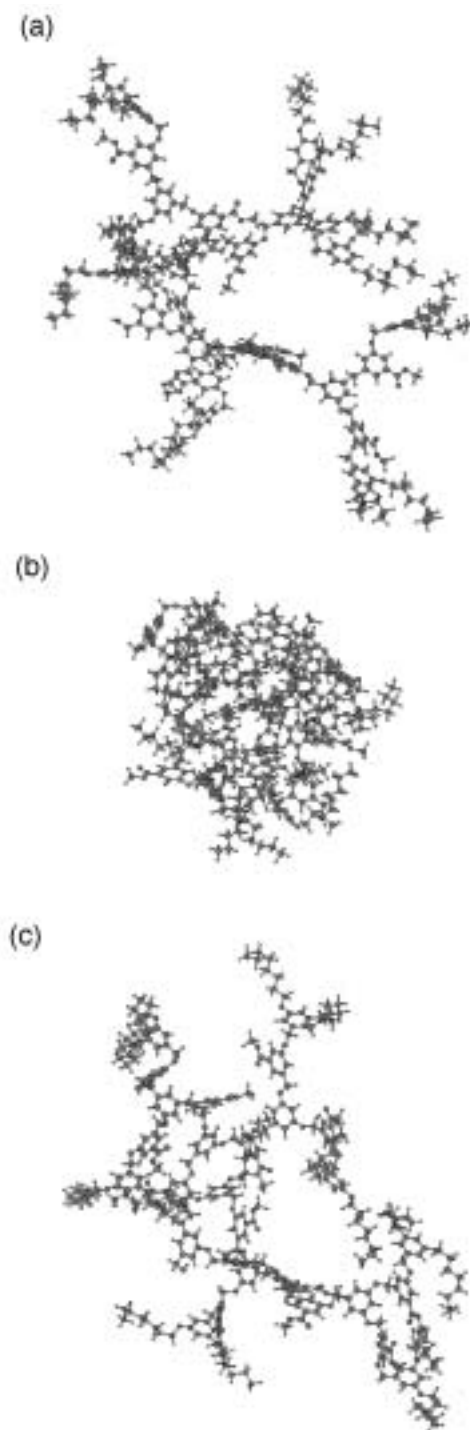


Figure 2. Ball-and-stick representations of the dendron, (a) before the molecular dynamics (MD) run, (b) after 100-ps MD without solvent, (c) after 100-ps MD with explicit solvent (CHCl_3).

IX-M Designing Artificial Photosynthesis at Molecular Dimensions

Photosynthesis is one of the finest piece of molecular machinery that Nature has ever created. Its ultrafast electron transfer and following well-organized sequence of chemical transformation have been, and will continue to be, challenging goals for molecular scientists. Our ultimate goal is to design artificial molecular systems that effect multiple chemical reactions triggered by light on the basis of molecular rationale.

IX-M-1 Synthesis of Dendrimer-Linked Porphyrins Bearing Multiple Quinone Moieties at Internal Positions

KIKUZAWA, Yoshihiro; ITO, Hajime; HINO, Takami; NAGATA, Toshi

By use of dendrons described above, we synthesized dendrimer-linked porphyrins bearing up to fourteen quinone moieties at internal positions of the dendrimer. The CV (cyclic voltammetry) and DPV (differential pulse voltammetry) measurements revealed that all the quinone moieties were simultaneously reduced at -1.18 V. The steady-state fluorescence spectra showed reduced emissions (10–15%), which recovered by chemical reduction of quinones by sodium dithionite.

The quinones in these compounds were quantitatively converted to hydroquinone disilyl ethers by irradiation of these compounds in the presence of PhSSiMe_3 . This suggests that even the quinones at the third-generation positions may accept electrons from the photoexcited porphyrin.

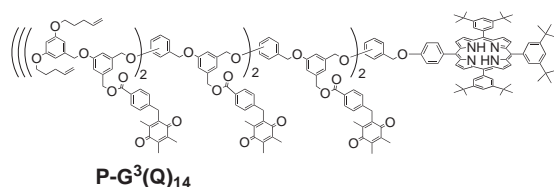


Figure 1. The structure of the quinone-dendrimer-linked porphyrins.

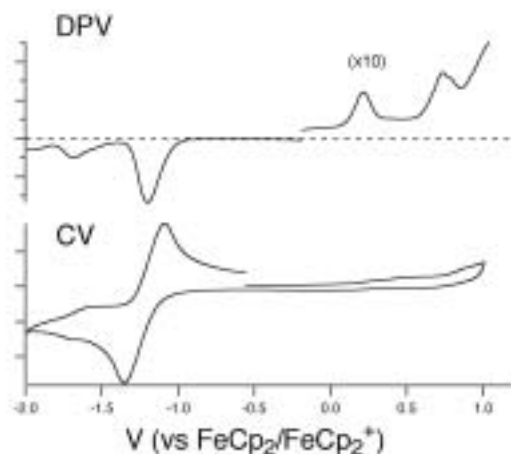


Figure 2. The CV and DPV voltammograms of the quinone-dendrimer-linked porphyrin zinc complex.

IX-N Photochemistry on Well-Defined Surfaces

Upon the irradiation of light in the wavelength range from visible to ultraviolet, a number of adsorbed molecules on metal surfaces reveal variety of photochemical processes, including photo-stimulated desorption, rearrangement of adsorbed states, photodissociation, and photo-initiated reactions with coadsorbates. A central and fundamental question in the surface photochemistry is to clarify how adsorbate-substrate systems are excited by photon irradiation. In addition, since photo-initiated reactions can be induced without any thermal activation of reactants, they may provide good opportunities for studying a new class of surface reactions that may not be induced thermally. We have studied photochemistry of various adsorption systems on well-defined metal and semiconductor surfaces mainly by temperature-programmed desorption (TPD), infrared reflection absorption spectroscopy (IRAS), x-ray photoelectron spectroscopy (XPS), work function measurements, near edge x-ray absorption fine structure (NEXAFS) and angular-resolved time-of-flight (TOF) mass spectrometry of photodesorbed species associated with pulsed laser irradiation. In this year, the photochemistry of alkane on Pt(111) and Cu(111) surfaces was studied mainly by TPD, XPS, and IRAS.

IX-O Ultrafast Dynamics at Well-Defined Surfaces

To understand the mechanism of surface photochemistry, it is vital to know how photoinduced electronic excitation induces adsorbate nuclear motions that ultimately lead to chemical reactions. We demonstrate the real-time observations of surface phonons and adsorbate-substrate vibrational modes by fs time-resolved second harmonics generation (TRSHG). If an excitation light pulse has a duration sufficiently shorter than a period of a vibrational mode or a phonon mode, it can excite the mode with a high degree of temporal and spatial coherence. This coherent nuclear motion modulates the second-order susceptibility $\chi^{(2)}$. Thus, by monitoring the intensity modulation of the second harmonics (SH) generation of a probe pulse, we can observe the evolution of the coherent nuclear motion subsequent to the electronic excitation at the surfaces.

IX-O-1 Direct Time-Domain Observation of Ultrafast Dephasing in Adsorbate-Substrate Vibration under the Influence of a Hot Electron Bath: Cs Adatoms on Pt(111)

WATANABE, Kazuya¹; TAKAGI, Noriaki¹;
MATSUMOTO, Yoshiyasu
(¹GUAS)

[*Phys. Rev. Lett.* **92**, 57401 (4 pages) (2004)]

Femtosecond time-resolved second harmonic generation has been used to observe vibrational wavepacket dynamics at a Cs-covered Pt(111) surface. The creation and dephasing of vibrational coherence are monitored *via* the intensity modulations in the second harmonic of probe pulses as a function of pump-probe delay. The TRSHG trace obtained from the clean surface shows an instantaneous sharp rise right after the excitation. This is followed by a fast decaying component ($t < 1$ ps) and a slowly decaying one persistent to the longest delay ($t = 6$ ps) of the measurements. When

the surface is covered with Cs, SH signals are enhanced by about 70 times and strongly modulated waveforms are superimposed on the TRSHG traces. The oscillatory signals are found in TRSHG signals upon the excitations at 580 and 800 nm, which are the manifestation of nuclear wavepacket dynamics on the surface. The Cs-coverage dependence studied in detail indicates that the wavepacket dynamics of Cs–Pt stretching modes and Pt surface phonon modes are responsible for the TRSHG signals. The cos-like initial phase of the oscillatory signals and the coverage dependence of the initial amplitude suggest that the vibrational coherence is associated with the resonant excitation between Cs-derived states in the quantum well of the Cs overlayer. The rate of Cs–Pt vibrational dephasing increases with the surface temperature. This behavior cannot be accounted for by the increasing contribution from hot bands of low frequency modes. Instead, pure dephasing caused by anharmonic coupling between Cs–Pt stretching and parallel modes in the Cs overlayer is likely the dominant mechanism for the vibrational dephasing.

IX-P Multiphoton Photoelectron Spectroscopy of Electronic States of Nano-Structured Materials on Surfaces

Electronic structure and excited state dynamics of nano-structured materials on surfaces are very important for

exploring their properties, thermal reactivity and nonthermal processes including photochemistry and photo-induced charge transfer. For this purpose, we performed multiphoton photoelectron spectroscopy with the fs time resolution. In this year we applied this method to thin films of 3,4,9,10-perylene tetracarboxylic dianhydride (PTCDA).

IX-P-1 Ultrafast Excited State Dynamics in 3,4,9,10-Perylene Tetracarboxylic Dianhydride (PTCDA) Thin Films

INO, Daisuke¹; WATANABE, Kazuya¹; TAKAGI, Noriaki¹; MATSUMOTO, Yoshiyasu (¹GUAS)

[*Chem. Phys. Lett.* **383**, 261–265 (2003)]

Ultrafast decay dynamics of the excited state in the

thin films of 3,4,9,10-perylene tetracarboxylic dianhydride (PTCDA) have been directly observed by using fs time-resolved two-photon photoelectron spectroscopy. The lifetimes were measured up to the excess energy of 2 eV above the S_1 state. The highly excited state presumably S_2 decays with $\tau = 70$ fs and S_1 with $\tau = 360 \pm 12$ fs. The lifetime in the S_1 manifold decreases with increase of excess energy, which manifests itself in a time-dependent energy shift of the photoelectron peak originated from the S_1 state.

IX-Q Chemistry of One-Dimensional Nano-Surface Compounds Studied by Scanning Tunneling Microscopy

The fluctuating configurations of low-dimensional structures can be thermodynamically favorable at finite temperatures, because the energy gain overcomes the energy cost that accompanies local structural fluctuation. In particular, one-dimensional (1D) systems have a propensity to be sensitive to these fluctuations as described by one of the maxims of condensed matter physics, *i.e.*, one chain does not make a crystal. Thus, the dynamical formation of active species and sites by these fluctuations is a key factor in establishing a microscopic model for chemical reactions at surfaces and nano-structured compounds.

IX-Q-1 Dynamic Formation of Reaction Sites at Nano-Structured One-Dimensional Surface Compounds

MATSUMOTO, Yoshiyasu; NAKAGOE, Osamu¹; WATANABE, Kazuya¹; TAKAGI, Noriaki¹ (¹GUAS)

[*Proc. SPIE* **5223**, 232–240 (2003)]

It is well known that the adsorption of O on Ag(110) results in the formation of quasi-1D structures, AgO chains, accompanied by the mass transfer of substrate atoms.

AgO chains arrange periodically to form $(n \times 1)$ ($n = 2 \sim 7$) depending on the fractional O coverage due to repulsive inter-chain interactions. Scanning tunneling microscopy is utilized to investigate the structural changes of AgO chains on clean and carbide-carbon

containing Ag(110) surfaces under UV photoirradiation and CO exposure. Although AgO chains are arranged with the (2×1) structure on both of the surfaces, AgO chains are bundled to make the (2×1) bands on the C-containing surface, whereas they make much larger domains on the entire surface of clean Ag(110). The photo-induced elimination of O in AgO chains occurs only on the C-containing surface. Kinetics of oxygen elimination by CO exposure are very different between the two surfaces. Oxygen coverage decreases steadily on the C-containing surface with CO exposure, whereas the reaction is accelerated in the lower O coverage range where AgO chains with $(n \times 1)$ ($n \geq 4$) configurations show significant structural fluctuation. Comparison between the two surfaces and simulations based on the Ising model indicate that the acceleration of the reaction originates from the dynamical formation of active O adatoms by fluctuation of AgO chains.

IX-R Adsorbate Structure and Surface Chemistry on Well-Defined Surfaces

Surface reactions have been playing an important role in production of many useful compounds and also fabrication of electronic devices. In particular, investigations on the structures of adsorbates and their reactivity are the first step for understanding more complicated catalytic reactions. We investigate surface reactions and kinetics

by means of various techniques including temperature-programmed desorption (TPD), x-ray photoelectron spectroscopy (XPS), ultraviolet photoelectron spectroscopy (UPS), work function measurements, Auger electron spectroscopy (AES), infrared reflection absorption spectroscopy (IRAS) and scanning tunneling microscopy (STM).

**IX-R-1 Reactivity of Molecular Oxygen:
Conversion of Methanol to Formate at Low
Temperatures on Pt(111)**

**SAWADA, Takeshi¹; LIU, Zhengxin²; TAKAGI,
Noriaki¹; WATANABE, Kazuya¹; MATSUMOTO,
Yoshiyasu**
(¹GUAS; ²System Engineers' Co.)

[*Chem. Phys. Lett.* **392**, 334–339 (2004)]

The oxidation of methanol by molecular oxygen on a Pt(111) surface has been investigated by infrared reflection absorption spectroscopy and X-ray photoelectron spectroscopy. Formate is produced when the surface coadsorbed with molecular oxygen and methanol is annealed to 70 K; the temperature is far much lower than the dissociation temperature of molecular oxygen on a clean Pt(111) surface. The attractive interaction between the coadsorbates is postulated to lower a dissociation barrier of molecular oxygen. When a methanol-precovered Pt(111) surface is exposed to O₂, the sticking probability of O₂ decreases with increase of surface temperature and the major product of methanol oxidation is changed from formate to CO.

IX-S Structures, Stabilities and Physicochemical Properties of Organometallic Hybrid Clusters

Recently, metal clusters have gained much attention because they exhibit novel physicochemical properties that are beyond the prediction made by a dimensional scaling of those of the corresponding bulk. In this regard, metal clusters protected by thiolates or stabilized by polymers are promising candidates for elementary units of nano-scale devices. Our interests are focused on the following issues on the organometallic hybrid clusters: (1) a large-scale preparation of the subnanometer-sized clusters, (2) development of size-selection method, (3) determination of chemical compositions of size-selected clusters (*i.e.* the numbers of metal atoms and organic molecules), and (4) elucidation of effect of the core size, core shape, and interaction with organic molecules on stabilities, electronic structures, and chemical properties.

IX-S-1 Magic-Numbered Au_n Clusters Protected by Glutathione Monolayers (*n* = 18, 21, 25, 28, 32, 39): Isolation and Spectroscopic Characterization

NEGISHI, Yuichi; TAKASUGI, Yoshimitsu¹;
SATO, Seiichi¹; YAO, Hiroshi¹; KIMURA,
Keisaku¹; TSUKUDA, Tatsuya
(¹Univ. Hyogo)

[*J. Am. Chem. Soc.* **126**, 6518–6519 (2004)]

Small gold clusters (< 1 nm) protected by glutathione (GSH) monolayer were fractionated into six components by polyacrylamide gel electrophoresis (PAGE) and their chemical compositions were investigated by electrospray ionization (ESI) mass spectroscopy. The results demonstrate isolation of a series of magic-numbered gold clusters, Au₁₈(SG)₁₁, Au₂₁(SG)₁₂, Au_{25±1}(SG)_{14±1}, Au₂₈(SG)₁₆, Au₃₂(SG)₁₈, and Au₃₉(SG)₂₃. Their optical absorption spectra are highly structured with clear absorption onsets, which shift toward higher energies with reduction of the core size. These molecular-like gold clusters exhibit visible photoluminescence. The results reported herein provide helpful guidelines or starting points for further experimental and theoretical studies on structures, stabilities and optical properties of small gold MPCs.

IX-S-2 Effect of Thiolate Ligation on Stabilization and Electronic Structures of Subnanometer-Sized Gold Clusters

NEGISHI, Yuichi; NOBUSADA, Katsuyuki;
TAKASUGI, Yoshimitsu¹; SATO, Seiichi¹; YAO,
Hiroshi¹; KIMURA, Keisaku¹; TSUKUDA, Tatsuya
(¹Univ. Hyogo)

Small gold clusters protected by *N*-(2-mercapto-propionyl)glycine (MPG) and mercaptosuccinic acid (MSA) were prepared and isolated into several components by high-resolution PAGE. Mass analysis shows that the core sizes of the monolayer-protected gold clusters (gold MPCs) preferentially formed are dependent on the thiolate structures. This finding suggests the completion of the protecting shell plays an important role in stabilizing the gold MPCs with specific core sizes. In other words, it may be possible to prepare gold MPCs with any desired core size by proper design of the

thiolate structures. Remarkable effect of thiolate ligation on the optical properties offers a new strategy toward fine-tuning of the fundamental properties of the MPCs through the degree of thiolate ligation as well as core size.

IX-S-3 Construction of Apparatus for Photodissociation and Surface-Induced Dissociation Studies of MPCs

NEGISHI, Yuichi; TSUKUDA, Tatsuya

Photo-dissociation and surface-induced dissociation of MPCs provide direct information on their thermodynamic stabilities. Such information also helps in the understanding of the origin of the preferential formation of certain-sized MPCs. Thus, we have improved our ESI-TOF mass spectrometer by introducing two components: a quadrupole ion trap and a reflectron coupled with an in-line MCP detector with a center hole. The continuous beam of the MPC ions formed in the ESI source is guided to the quadrupole ion trap. The ions accumulated in the trap are extracted into a primary TOF mass spectrometer typically operated at 10 Hz. The mass-selected cluster ions are irradiated by a pulsed laser or allowed to collide with the solid surface mounted at the end of the reflectron. The fragment ions generated are detected by a secondary TOF mass spectrometer.

IX-S-4 Construction of Low-Temperature Optical Spectroscopy System

NEGISHI, Yuichi; TSUNOYAMA, Hironori;
TSUKUDA, Tatsuya

We have demonstrated that subnanometer-sized gold clusters exhibit clear structures in their optical spectra even at room temperature. In order to minimize the influence from vibration excitation of internal modes and/or isomers (if present), the measurement at low temperature is required. The system under construction is composed of a sample holder supported on a cold head (~22 K), a vacuum chamber, and a turbo-molecular pump. The system can be coupled to a spectrophotometer (HITACHI, U-2010) or a spectrofluorometer (JASCO, FP-6600) to obtain optical data of the neat film of the clusters.

IX-S-5 Heat Induced Long-Range Ordering of Small Gold Nanoparticles with Tunable Interparticle Spacings

KANEHARA, Masayuki¹; KODZUKA, Etsushi¹;
NEGISHI, Yuichi; TSUKUDA, Tatsuya;
TERANISHI, Toshiharu¹
(¹Univ. Tsukuba)

The monodisperse Au nanoparticles smaller than 2 nm were prepared by the reduction of HAuCl₄·4H₂O in DMF/H₂O in the presence of a series of ligands, 2,6-bis(1'-(*n*-thioalkyl)benzimidazol-2-yl)pyridine (TC_{*n*}BIP, *n* = 8, 10, 12), and formed hexagonal close packed (*hcp*) two-dimensional (2D) superlattices with tunable interparticle spacings from 1.9 to 2.5 nm by the ligand length. Then we present the new methodology to fabricate the long range ordered 2D superlattices of 1.5-nm Au nanoparticles at the air-water interface, which includes a heat-induced rearrangement of *hcp* domains into long range ordered *hcp* superlattices stabilized by interligand π - π interaction. The large-scale *hcp* 2D superlattices of 1.5-nm Au nanoparticles were obtained, and advantageously transferable onto any substrate.

IX-S-6 Colloidal Gold Nanoparticles as Catalyst for Carbon-Carbon Bond Formation: Application to Aerobic Homocoupling of Phenylboronic Acid in Water

TSUNOYAMA, Hironori; SAKURAI, Hidehiro;
ICHIKUNI, Nobuyuki¹; NEGISHI, Yuichi;
TSUKUDA, Tatsuya
(¹Chiba Univ.)

[*Langmuir* **20**, 11293–11296 (2004)]

Gold nanoparticles ($\phi < 2$ nm) stabilized by poly(*N*-vinyl-2-pyrrolidone) (Au:PVP NPs) were prepared by reduction of AuCl₄⁻ with NaBH₄ in the presence of PVP and characterized via array of methods including optical absorption spectroscopy, TEM, XRD, XANES, EXAFS, and XPS. It is found for the first time that the Au:PVP NPs act as catalyst toward homocoupling reactions of phenylboronic acid in water under aerobic conditions. Suppression of the biphenyl formation under anaerobic condition indicates that molecular oxygen dissolved in water is intimately involved in the coupling reactions. Effect of the particle size and the PVP coordination upon the catalytic activity is discussed.

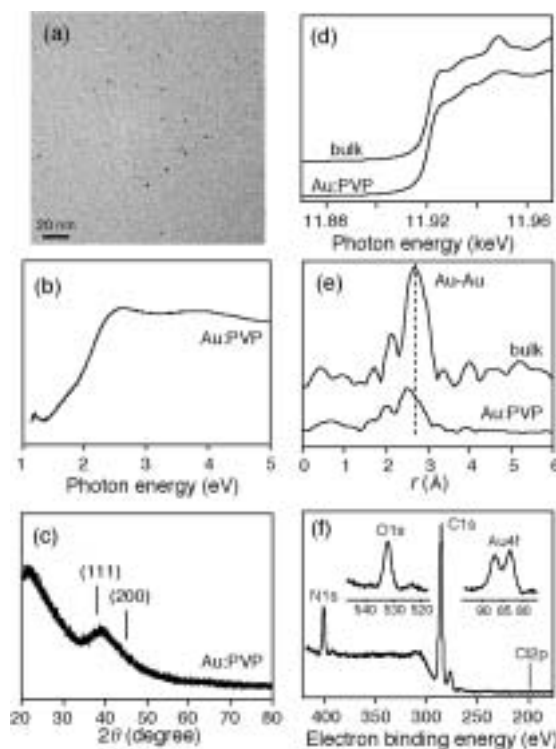
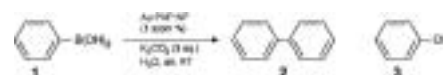


Figure 1. (a) TEM image, (b) optical absorption spectrum, (c) XRD profile, (d) Au L₃-edge XANES, (e) FT-EXAFS, (f) XPS of Au:PVP(K-30).

Table 1. Homocoupling Reactions of Phenylboronic Acid in Water Catalyzed by Au:PVP NPs^a.



entry	catalyst	yield (%) ^b			d (nm) ^d
		1 ^c	2	3	
1	Au:PVP(K-15)	16	62	22	3.1±0.7
2	Au:PVP(K-30)	3	72	23	2.9±0.4
3	Au:PVP(K-90)	trace	64	35	3.1±0.5
4 ^e	Au:PVP(K-30)	>99	trace	trace	–
5	recovered from #2 ^f	26	61	13	3.4±0.5
6	recovered from #5 ^f	43	49	8	3.4±0.6

^aThe reactions were carried out at room temperature under air for 24 h. ^bEstimated from NMR analysis. ^cDetected as anhydride. ^dParticle diameter after the reaction determined by TEM measurement. ^eThe reaction was carried out under nitrogen. ^fThe Au:PVP NPs were collected by centrifugal ultrafiltration by a filter with 10 kDa cutoff.

IX-S-7 Fabrication of Model Catalytic System by Use of Monolayer-Protected Metal Clusters as Precursor

TSUNOYAMA, Hironori; NEGISHI, Yuichi;
TSUKUDA, Tatsuya

Metal clusters supported on a surface have been regarded as an ideal model for the study of heterogeneous catalysts.¹⁾ In these studies, metal clusters with a given size were softly deposited on the surface, and

the catalytic activity was investigated as a function of the cluster size. However, following difficulties are encountered in this approach: (1) the clusters tend to aggregate at high coverage, (2) the structures of the clusters deposited on a surface may not be uniform because of isomers present in the beam or surface-induced structural rearrangement. In order to circumvent these difficulties, we have been developing a new scheme to fabricate an ordered array of size-selected metal clusters. An ordered array of size-selected MPCs is transferred to a solid substrate by using a Langmuir-Brodgett technique. As an initial step, we prepared the monolayer of alkanethiolate-protected gold clusters on a carbon-coated copper grid. In the monolayer obtained, the gold MPCs are arranged regularly with interparticle distance determined by the thickness of the thiolate monolayer.²⁾ The substrate is subsequently transferred into a UHV chamber which accommodates a magnetron-type plasma source. The organic layer of the MPCs is etched by exposure of the oxygen and/or hydrogen plasma. The structures of the resulting clusters are characterized by XPS and AFM. The activity of the model catalysts thus prepared is investigated in situ by means of thermal desorption spectroscopy.

References

- 1) A. Sanchez, S. Abbet, U. Heiz, W. -D. Schneider, H. Hakkinen, R. N. Barnett and U. Landman, *J. Phys. Chem. A* **103**, 9573 (1999).
- 2) P. Liljeroth, D. Vanmaekelbergh, V. Ruiz, K. Kontturi, H. Jiang, E. Kauppinen and B. M. Quinn, *J. Am. Chem. Soc.* **126**, 7126 (2004).

IX-T Fundamental Study on Electrostatic Manipulation of Biomolecules and Its Application to Gene Analysis

Since conventional DNA sequencing method can determine up to 1000 base pairs at one time, longer DNA must be cut into small fragments. However, order information among these fragments is inevitably lost resulting in tremendous post sequencing process to do a puzzle. To cope with the problem, we have studied DNA sequencing method based on one-by-one DNA handling. The method includes (1) electrostatic manipulation of genomic DNA, (2) fixation in a stretched form, (3) cut from the terminus, (4) recovery and amplification of the fragments.

IX-T-1 On-Demand Mixing Droplet Spotter for Preparing Picoliter Droplets on Surfaces

YOGI, Osamu¹; KAWAKAMI, Tomonori¹; MIZUNO, Akira
(¹Hamamatsu Photonics K. K.)

[*Anal. Chem.* **76**, 2991–2996 (2004)]

An on-demand mixing droplet spotter for generating and mixing picoliter droplet has been developed for ultrasmall reaction vessels. The droplets were generated by applying a ~500 V, ~2 ms pulsed voltage to the tips of capillary tubes (o.d. ~20 μm ; i.d. ~12 μm) filled with solution. The mixing process was achieved using electrostatic force. The initial droplet was formed by applying the pulsed voltage between one capillary and the substrate, and the second jet of the other solution was generated from the other capillary and collided with the initial droplet automatically because the electric field lines concentrated on the initial droplet. Using this mixing process, a microarray having a concentration gradient was obtained by spotting ~6 pL droplets on a surface with a density of one spot per $75 \times 75 \mu\text{m}^2$.

IX-T-2 Ice-Water Interface Migration by Temperature Controlling for Stretching of DNA Molecules

KOMATSU, Jun¹; NAKANO, Michihiko¹; KURITA, Hirofumi¹; TAKASHIMA, Kazunori¹; KATSURA, Shinji¹; MIZUNO, Akira²
(¹Toyohashi Univ. Tech.; ²IMS and Toyohashi Univ. Tech.)

[*J. Biomol. Struct. Dyn.* accepted]

This report shows a new DNA stretching method using migration of an ice-water interface. DNA molecules were stretched accompanying the migration of the solid-liquid interface and immobilized in frozen area. This simple method needs no chemical modification to keep DNA in the stretched form. For full stretching of DNA molecules, one terminus of the DNA molecules were anchored on silanized substrate. The anchored DNA molecules were stretched by freezing the DNA solution. The stretched DNA molecules were observed after sublimation of the frozen solution keeping its stretched form on silanized surface which had no attractive interaction with DNA molecules except for the SH-modified terminus in solution. An infrared (IR) laser beam was introduced to a frozen DNA solution

through an objective lens for local area melting of the solution. Scanning of the laser irradiation caused stretching and enclosing of DNA molecules in the frozen area followed by migration of the solid-liquid interface.

IX-T-3 Activation of Restriction Enzyme by Electrochemically Released Magnesium Ion

KATSURA, Shinji¹; HARADA, Noriaki¹; MAEDA, Yukihiro¹; KOMATSU, Jun¹; MATSUURA, Shun-ichi¹; TAKASHIMA, Kazunori¹; MIZUNO, Akira²
(¹Toyohashi Univ. Tech.; ²IMS and Toyohashi Univ. Tech.)

[*J. Biosci. Bioeng.* accepted]

Observation and cutting of DNA molecules at intended positions permit several new experimental methods that are completely different from conventional molecular biology methods; therefore several cutting methods have been proposed and studied. In this paper, a new cutting method for a DNA molecule by localizing the activity of a restriction enzyme is presented. Since most restriction enzymes require magnesium ions for their activation, local restriction enzyme activity can be controlled by the local concentration of magnesium ions. Applying a dc voltage to a needle electrode of metallic magnesium made it possible to control the local magnesium ion concentration at the tip of the needle. The restriction enzyme was activated only when magnesium ions were electrochemically supplied.

IX-U Electronic Structure and Collision Dynamics of Atoms and Molecules Studied by Electron Impact at Large Momentum Transfer

Binary (e,2e) or electron momentum spectroscopy (EMS) is a high-energy electron-impact ionization experiment in which kinematics of all the electrons are fully determined by coincident detection of the two outgoing electrons. The method enables us to look at individual molecular orbitals in momentum space, based on the so-called electron Compton scattering. However, EMS has long been plagued by the fact that the present experiments measure averages over all orientations of gaseous targets. The spherical averaging results in enormous loss of versatile information on electronic structure, in particular that on anisotropy of the target wavefunction. Consequently, one must be content to use EMS only as a stringent test for the target wavefunction model employed. Under these historical circumstances, we have successfully developed an electron-electron-fragment ion triple coincidence apparatus that makes it possible to carry out molecular frame EMS experiments for the first time, opening up the possibilities for detailed studies of bound electronic wavefunctions of molecules.

IX-U-1 (e,2e) Ionization-Excitation of H₂

**TAKAHASHI, Masahiko¹; KHAJURIA, Yugal;
UDAGAWA, Yasuo²**

(¹IMS and Tohoku Univ.; ²Tohoku Univ.)

[*Phys. Rev. A* **68**, 042710 (7 pages) (2003)]

Binary (e,2e) measurements are reported for simultaneous ionization-excitation processes of H₂. The experiments were performed at impact energies of 1200, 1600 and 2000 eV using an energy- and momentum-dispersive spectrometer. Momentum profiles for transitions to the 2s σ_g and 2p σ_u excited final ion states are presented as normalized intensities relative to the cross section of the primary ionization to the 1s σ_g ground ion state. The results are compared with theoretical calculations of Lermer *et al.* [*Phys. Rev. A* **56**, 1393 (1997)] using the first-order plane-wave impulse approximation. Certain features of the discrepancies between experiment and theory can be explained by incorporating contributions from the second-order two-step mechanisms into the (e,2e) cross sections. Furthermore, the present results suggest that 2s σ_g and 2p σ_u cross sections approach their high-energy limits in different ways.

IX-U-2 Electron Momentum Spectroscopy of N₂O

**KHAJURIA, Yugal; TAKAHASHI, Masahiko¹;
UDAGAWA, Yasuo²**

(¹IMS and Tohoku Univ.; ²Tohoku Univ.)

[*J. Electron Spectrosc. Relat. Phenom.* **133**, 113–121 (2003)]

An electron momentum spectroscopy study of the outer valence orbitals of N₂O is reported. The experiments were performed at impact energies of 1000, 1200, 1600 and 1800 eV by using a recently developed multi-channel (e,2e) spectrometer. The experimental momentum profiles are compared with each other to examine their impact energy dependence. The results are used for comparisons with Hartree-Fock (HF) and density func-

tional theory (DFT) calculations using various basis sets. The DFT and HF calculations with large basis sets are in good agreement with the measured electron momentum profiles, with the exception of that of the 6s orbital for which the HF method underestimates the cross sections in the low momentum region.

IX-U-3 Triple Differential Cross-Section of Ne(2s²) in Coplanar to Perpendicular Plane Geometry

**CHEN, Li Q.¹; KHAJURIA, Yugal; CHEN, Xian J.¹;
XU, Ka Z.¹**

(¹USTC)

[*Eur. Phys. J. D* **26**, 141–146 (2003)]

The distorted wave Born approximation (DWBA) with spin average static exchange potential has been used to calculate the triple differential cross sections (TDCSs) for Ne(2s²) ionization by electron impact in the coplanar to perpendicular plane geometry at 110.5 eV incident energy. The present theoretical results at gun angles $\Psi = 0^\circ$ (coplanar symmetric geometry) and $\Psi = 90^\circ$ (perpendicular plane geometry) are in satisfactory agreement with the available experimental data. A deep interference minimum appears in the TDCS in the coplanar symmetric geometry and a strong peak at a scattering angle $\xi = 90^\circ$ caused by the single collision mechanism has been observed in the perpendicular plane geometry. The TDCSs at the gun angles $\Psi = 30^\circ$, and $\Psi = 60^\circ$ are predicted.

IX-U-4 A High Sensitivity Electron Momentum Spectrometer with Two-Dimensional Detectors and Electron Momentum Distributions of Several Simple Molecules

TAKAHASHI, Masahiko¹; UDAGAWA, Yasuo²
(¹IMS and Tohoku Univ.; ²Tohoku Univ.)

[*J. Electron Spectrosc. Relat. Phenom.* **137-40**, 387–391 (2004)]

Electron momentum spectroscopy (EMS) makes it

possible to examine orbital patterns of individual molecular orbitals in momentum space. A new spectrometer for electron-electron coincidence experiments for EMS has been developed to obtain orbital patterns quantitatively. Using a spherical analyzer and position-sensitive two-dimensional detectors combined with fast electronics, simultaneous measurements of energy and angular correlations between the two outgoing electrons can be made. This spectrometer features high sensitivity and an ease of changing impact energies. Details of the apparatus are described and impact energy dependence of electron momentum distributions of the HOMO of H₂ and biacetyl are compared.

IX-U-5 Practical Means for the Study of Electron Correlation in Atoms

VAN BOEYEN, Roger W.¹; WATANABE, Noboru²; DOERING, John P.¹; MOORE, John H.³; COPLAN, Michael A.³
(¹Johns Hopkins Univ.; ²IMS and Tohoku Univ.; ³Univ. Maryland)

[*Phys. Rev. Lett.* **92**, 223202 (4 pages) (2004)]

Electron correlation is basic to the understanding of a diverse range of physical and chemical phenomena, yet, there have been no direct measurements of the correlated motion of electrons. Measurement of the correlated momenta of atomic electrons is possible via electron-impact double ionization provided that the ionizing collisions are both impulsive and binary, and the three-body scattering mechanism is known. The results reported here satisfy these conditions, and a practical means for the study of atomic electron correlation through measurement of two-electron momentum densities is presented.

IX-U-6 Development and Use of a Multichannel (e,2e) Spectrometer for Electron Momentum Densities of Molecules

TAKAHASHI, Masahiko¹; UDAGAWA, Yasuo²
(¹IMS and Tohoku Univ.; ²Tohoku Univ.)

[*J. Phys. Chem. Solids* **65**, 2055–2059 (2004)]

We have developed an (e,2e) spectrometer with the introduction of modern multiparameter techniques. In particular, the high sensitivity achieved by simultaneous detection in energy and momentum is remarkable, opening up the possibilities of more precise and more advanced studies on the electronic structure of atoms and molecules. To illustrate some of the features, an overview of our recent results is presented. Highlights are applications to collision dynamics of H₂ and development of a method for a complete three-dimensional mapping of electron momentum densities in gaseous molecules. Both of these studies are based on the high sensitivity of the spectrometer.

IX-U-7 Electron Momentum Spectroscopy of Valence Satellites of Neon

WATANABE, Noboru¹; KHAJURIA, Yugal;
TAKAHASHI, Masahiko¹; UDAGAWA, Yasuo²
(¹IMS and Tohoku Univ.; ²Tohoku Univ.)

[*J. Electron Spectrosc. Relat. Phenom.* in press]

Electron momentum spectroscopy (EMS) study of the neon valence satellites is reported. The experiments were performed at impact energies of 1250, 1450 and 1670 eV using a multichannel spectrometer that features high sensitivity. Binding energy spectra up to 100 eV and momentum profiles for the 2p⁻¹ and 2s⁻¹ primary transitions as well as the satellites are presented. The results are used to examine impact energy dependence of the relative intensities and shapes of the satellite momentum profiles. The results are also used to determine symmetries and spectroscopic factors of the satellites, and are compared with the previous experiments by EMS and photoelectron spectroscopy and sophisticated theoretical calculations. The present study has largely resolved controversies in the previous studies.

IX-U-8 Observation of Molecular Frame (e,2e) Cross Section Using an Electron-Electron-Fragment Ion Triple Coincidence Apparatus

TAKAHASHI, Masahiko¹; WATANABE, Noboru¹; KHAJURIA, Yugal; NAKAYAMA, Kazuya²; UDAGAWA, Yasuo²; ELAND, John H. D.³
(¹IMS and Tohoku Univ.; ²Tohoku Univ.; ³IMS and Oxford Univ.)

[*J. Electron Spectrosc. Relat. Phenom.* **141**, 83–93 (2004)]

An apparatus for electron-electron-fragment ion triple coincidence experiments has been developed to examine binary (e,2e) scattering reaction in the molecular frame. In the axial recoil limit of fragmentation of the residual ion, measurements of vector correlations among the three charged particles are equivalent to (e,2e) experiments with fixed-in-space molecules. Details and performance of the apparatus are reported, together with preliminary result of collision dynamics study on ionization-excitation processes of fixed-in-space H₂ molecules. We believe that this is the first observation of molecular frame (e,2e) cross sections.

IX-U-9 (e,3e) Collisions on Mg in the Impulsive Regime Studied by Second Born Approximation

WATANABE, Noboru¹; COOPER, John W.²; VAN BOEYEN, Roger W.³; DOERING, John P.³; MOORE, John H.²; COPLAN, Michael A.²
(¹IMS and Tohoku Univ.; ²Univ. Maryland; ³Johns Hopkins Univ.)

[*J. Phys. B: At., Mol. Opt. Phys.* submitted]

Five-fold differential cross sections for electron-impact double ionization of the 3s electrons of magnesium have been calculated in the second Born approximation in the impulsive regime. Comparing

these results with calculations carried out in the first Born approximation demonstrates the dominant contribution of the second Born term. The second Born calculation shows that contribution of the two-step 2 (TS2) process becomes large under the condition where sequential binary collisions on the Bethe ridge can occur. The effect of electron correlation in the initial target state is also examined by using a configuration interaction wavefunction.

IX-U-10 Molecular Frame (e,2e) Cross Sections Observed for Ionization-Excitation Processes of H₂

TAKAHASHI, Masahiko¹; WATANABE, Noboru¹; KHAJURIA, Yugal; UDAGAWA, Yasuo²; ELAND, John H. D.³

(¹IMS and Tohoku Univ.; ²Tohoku Univ.; ³IMS and Oxford Univ.)

[*Phys. Rev. Lett.* submitted]

We report on first kinematically complete experiment of (e,2e) scattering by molecules using the electron-electron-fragment ion triple coincidence technique. Vector correlations among the two outgoing electrons and the fragment ion have been measured for ionization-excitation processes of H₂. The results are used to obtain (e,2e) cross section in the molecular frame and to observe the collision stereodynamics, the phenomenon that has never been explored so far.

IX-U-11 Double Ionization of He by (e,3-1e) at Large Momentum Transfer

KHAJURIA, Yugal; WATANABE, Noboru¹; TAKAHASHI, Masahiko¹; UDAGAWA, Yasuo²; POPOV, Yuri V.³; KOZAKOV, Konstantin A.³; VINITSKY, Pavel S.³; CHULUUNBAATAR, Ochbadrakh⁴

(¹IMS and Tohoku Univ.; ²Tohoku Univ.; ³Moscow State Univ.; ⁴JINR)

[*Phys. Rev. A* to be submitted]

The present (e,3-1e) experiment aims at investigating double ionization at large momentum transfer that would provide direct information on electron correlation in the target initial state. The (e,3-1e) method involves coincident detection of the two fast outgoing electrons while keeping the slow outgoing electron undetected. It has been found from comparison between experiment and theory that (e,3-1e) momentum profile is very sensitive to the target electron correlation, as expected. In fact, the experimental profile shape is reproduced

well by first Born calculations using highly correlated wavefunctions. However, there is noticeable intensity difference between experiment and theory. The calculation underestimates the experimental cross sections significantly by a few times of magnitude, suggesting need of incorporating higher Born terms and/or more accurate description of correlated electron pair in helium.

IX-U-12 (e,2e) Study on Distorted Wave Effects in the Xe 4d⁻¹ Ionization Process

KHAJURIA, Yugal; WATANABE, Noboru¹;

YOSHINO, Tae²; SAKAI, Yasuhiro²;

TAKAHASHI, Masahiko¹; UDAGAWA, Yasuo³

(¹IMS and Tohoku Univ.; ²Toho Univ.; ³Tohoku Univ.)

[*J. Phys. B: At., Mol. Opt. Phys.* to be submitted]

Momentum profiles for the Xe 4d⁻¹ ionization process have been studied by means of binary (e,2e) at various impact energies. The results are found to exhibit considerable intensity near the momentum origin that the plane-wave impulse approximation (PWIA) theory can not predict. The discrepancy from PWIA is substantially reduced by distorted-wave theory. Furthermore, momentum profiles for the core 4d_{3/2} and 4d_{5/2} orbitals of Xe are compared with associated theoretical momentum profiles generated using Dirac-Fock wavefunctions to investigate relativistic effects in the ionization process.

IX-U-13 The Impact Energy Dependence of Momentum Profile of Acetone and Comparison with Theory at Its High-Energy Limit

CHO, Tegyon¹; KHAJURIA, Yugal; WATANABE, Noboru²; TAKAHASHI, Masahiko²; UDAGAWA, Yasuo¹

(¹Tohoku Univ.; ²IMS and Tohoku Univ.)

[*J. Phys. B: At., Mol. Opt. Phys.* to be submitted]

We report an electron momentum spectroscopy study of the outermost orbital of acetone. The experiments were performed at impact energies of 800, 1200, 1600 and 2000 eV by using a recently developed multichannel (e,2e) spectrometer. The results at 2000 eV are compared with plane-wave impulse approximation calculations using Hartree-Fock (HF) and density functional theory (DFT). While the DFT calculations reproduce the observations better than HF, noticeable discrepancy between experiment and theory still remains.

IX-V Electronic Structure and Collision Dynamics of Atoms and Molecules Studied by Photon Impact

The group takes another, photon-impact, approach to issues of electronic structure and collision dynamics, since photon-impact and electron-impact or photoelectric effects and Compton scattering are complementary to each other.

IX-V-1 N 1s Photoionization Cross Sections of the NO Molecules in the Shape Resonance Region

HOSAKA, Kouichi¹; ADACHI, Junichi^{1,2};
TAKAHASHI, Masahiko³; YAGISHITA, Akira^{1,2}
(¹Univ. Tokyo; ²KEK-PF; ³IMS and Tohoku Univ.)

[*J. Phys. B: At., Mol. Opt. Phys.* **36**, 4617–4629 (2003)]

The N 1s partial photoionization cross sections of NO leading for the ³Π and ¹Π ionic states have been measured in the shape resonance region for the first time. The twin local maxima in the cross sections have been tentatively assigned, based on the simple models for the photoabsorption intensities and for the branching ratio of the ³Π and ¹Π ionic states from the σ* shape resonance state.

IX-V-2 Shape-Resonance-Enhanced Vibrational Effects in the Angular Distributions of C 1s Photoelectrons from Fixed-in-Space CO Molecules

ADACHI, Junichi^{1,2}; HOSAKA, Kouichi¹;
FURUYA, Shuusaku³; SOEJIMA, Kouich³;
TAKAHASHI, Masahiko⁴; YAGISHITA, Akira^{1,2};
SEMENOV, Sergei K.⁵; CHEREPKOV, Nikolai A.⁵
(¹Univ. Tokyo; ²KEK-PF; ³Niigata Univ.; ⁴IMS and Tohoku Univ.; ⁵State Univ. Aerospace Instrum.)

[*Phys. Rev. Lett.* **91**, 163001 (4pages) (2003)]

Angular distributions of C1s photoelectrons from fixed-in-space CO molecules have been measured with vibrational resolution. A strong dependence of the angular distributions on the vibrational states of the residual molecular ion has been found for the first time in the region of the shape resonance. Calculations in the relaxed core Hartree-Fock approximation have reproduced the angular distributions fairly well in the general shapes of the angular distributions due to the correct description of nuclear motion as an average of the internuclear-distance-dependent dipole amplitudes.

IX-V-3 Photoelectron-Photoion-Photoion Coincidence in Ar Dimers

FANIS, Albert De^{1,2}; OURA, Masaki³; SAITO, Norio⁴; MACHIDA, Masatake^{3,5}; NAGOSHI, Mitsuru⁵; KNAPP, Alexandra⁶; NICKLES, Jurgen⁶; CZASCH, Achim⁶; DÖRNER, Reinhard⁶; TAMENORI, Yusuke¹; CHIBA, Hisashi⁷; TAKAHASHI, Masahiko⁷; ELAND, John H. D.⁸;

UEDA, Kiyoshi²

(¹JASRI; ²Tohoku Univ.; ³RIKEN; ⁴Natl. Metrology Inst.; ⁵Himeji Inst. Tech.; ⁶Univ. Frankfurt; ⁷IMS and Tohoku Univ.; ⁸Oxford Univ.)

[*J. Phys. B: At., Mol. Opt. Phys.* **37**, L1–L8 (2004)]

Photoelectron-photoion-photoion coincidence momentum imaging was applied to study 2p photoemission from Ar dimers. We present measurements of the kinetic energy released in fragmentation of Ar₂⁺⁺, angular distributions of energetic fragments, angular distributions of photoelectrons in the laboratory frame and in the molecular frame. The mean kinetic energy of fragment Ar⁺ ions, 2.2 eV, is larger than the value estimated from the Coulomb explosion model with the equilibrium Ar–Ar distance. No significant differences between the photoelectron angular distributions of monomers and dimers can be found in the laboratory frame. The photoelectron angular distributions of dimers in the molecular frame show a minimum for electron emission along the dimer axis at low energies (1.2 and 3.4 eV) and become isotropic at higher kinetic energies.

IX-V-4 Multiplet-Specific N 1s Photoelectron Angular Distributions from the Fixed-in-Space NO Molecules

HOSAKA, Kouichi¹; ADACHI, Junichi^{1,2};
TAKAHASHI, Masahiko³; YAGISHITA, Akira^{1,2};
LIN, Ping⁴; LUCCHESI, Robert R.⁴
(¹Univ. Tokyo; ²KEK-PF; ³IMS and Tohoku Univ.; ⁴Texas A&M Univ.)

[*J. Phys. B: At., Mol. Opt. Phys.* **37**, L49–L55 (2004)]

Angular distributions of multiplet-specific N 1s photoelectrons from the fixed-in-space NO molecules have been measured for the first time. The dynamics of the σ* shape resonance appeared in the channel leading to the ³Π and ¹Π ionic states has been made clear from the analyses of the angular distributions. Multiplet-specific multichannel calculations have reproduced the observed angular distributions fairly well.

IX-V-5 Angular Distributions of Vibrationally Resolved C 1s Photoelectrons from Fixed-in-Space CO Molecules: Vibrational Effect in the Shape-Resonant C 1s Photoionization of CO

ADACHI, Junichi^{1,2}; HOSAKA, Kouichi¹;
FURUYA, Shuusaku³; SOEJIMA, Kouich³;
TAKAHASHI, Masahiko⁴; YAGISHITA, Akira^{1,2};

SEMENOV, Sergei K.⁵; CHEREPKOV, Nikolai A.⁵
(¹Tokyo Univ.; ²KEK-PF; ³Niigata Univ.; ⁴IMS and
Tohoku Univ.; ⁵State Univ. Aerospace Instrum.)

[*J. Electron Spectrosc. Relat. Phenom.* **137-40**, 243–248
(2004)]

We have measured molecular-frame photoelectron angular distributions (MF-PAD) for the vibrationally resolved C1s photoelectron from CO molecule in the σ shape resonance region. The MF-PAD's for the $v_f = 0, 1,$ and 2 levels in the C1s $\rightarrow \epsilon\ell\sigma$ channel are apparently different each other at each incident photon energy. These MF-PAD's agree with the present theoretical results from the averaging the nuclear distance dependent dipole matrix elements with the relaxed core Hartree-Fock calculations. The present results show that the internuclear distance dependences of the phase and of the magnitude of the dipole matrix element play a crucial role in the C1s photoionization of CO.

IX-V-6 Coulomb Hole in N₂, CO and O₂ Deduced from X-Ray Scattering Cross Sections

**WATANABE, Noboru¹; KAMATA, Yohei²;
YAMAUCHI, Kota²; UDAGAWA, Yasuo²;
MÜLLER, Thomas³**
(¹IMS and Tohoku Univ.; ²Tohoku Univ.; ³Res. Cent.
Jülich)

[*Mol. Phys.* **102**, 649–657 (2004)]

Accurate total (elastic + inelastic) x-ray scattering cross sections $\sigma_{ee}(q)$ of N₂, CO and O₂ were measured by the use of the energy dispersive method up to a momentum transfer of $q = 12$ a.u. The radial electron pair distribution function $P(r_{12})$ was extracted from the cross sections. The Coulomb hole, defined as the difference between the exact $P(r_{12})$ and the corresponding function evaluated at Hartree-Fock limit, has been derived from experimental data for the first time. Comparison of multi reference configuration interaction (MRCI) and averaged quadratic coupled cluster (MR-AQCC) calculations indicate substantial shortcomings of MRCI due to the lack of size extensivity. The overall agreement with experiment is good but some differences between the theoretical and experimental results remain.

IX-V-7 Absolute Surface Coverage Measurement Using a Vibrational Overtone

**PIPINO, Andrew C. R.¹; HOEFNAGELS, Johan P. M.²;
WATANABE, Noboru³**
(¹Natl. Inst. Standards Tech.; ²Eindhoven Univ. Tech.;
³IMS and Tohoku Univ.)

[*J. Chem. Phys.* **120**, 2879–2888 (2004)]

Determination of absolute surface coverage with sub-monolayer sensitivity is demonstrated using evanescent-wave cavity ring-down spectroscopy (EW-CRDS) and conventional CRDS by employing conservation of the absolute integrated absorption intensity between gas

and adsorbed phases. The first C–H stretching overtones of trichloroethylene (TCE), *cis*-dichloroethylene, and *trans*-dichloroethylene are probed using the idler of a seeded optical parametric amplifier having a 0.075 cm⁻¹ line width. Polarized absolute adsorbate spectra are obtained by EW-CRDS using a fused-silica monolithic folded resonator having a finesse of 28500 at 6050 cm⁻¹, while absolute absorption cross sections for the gas-phase species are determined by conventional CRDS. A measure of the average transition moment orientation on the surface, which is utilized for the coverage determination, is derived from the polarization anisotropy of the surface spectra. Coverage measurement by EW-CRDS is compared to a mass-spectrometer-based surface-uptake technique, which we also employ for coverage measurements of TCE on thermally grown SiO₂ surfaces. To assess the potential for environmental sensing, we also compare EW-CRDS to optical waveguide techniques developed previously for TCE detection.

IX-V-8 Direct Observation of a Symmetry Lowering in Core-Electron Ionization for Highly Symmetric Molecules

**HOSAKA, Kouichi¹; ADACHI, Junichi^{1,2};
GOLOVIN, Alexander V.²; TAKAHASHI,
Masahiko³; TERAMOTO, Takahiro¹;
WATANABE, Noboru³; YAGISHITA, Akira^{1,2}**
(¹Tokyo Univ.; ²KEK-PF; ³IMS and Tohoku Univ.)

(Nature to be submitted)

The Jahn-Teller theorem governs stable structures of crystalline solids and molecules with an element of symmetry. This is because electro-vibrational (vibronic) coupling splits degenerate adiabatic-states by lowering the symmetry. The symmetry lowering occurs quite often in the ionization of a core electron of equivalent constituent-atoms for highly symmetric molecules since the core-hole states of those molecules are generally quasi-degenerate and therefore couple over non-totally symmetric vibrational modes. Such couplings, referred as quasi-Jahn-Teller couplings, have been clearly investigated for the most basic example of CO₂; the relation between the symmetry lowering and core-hole localization has been proved. The symmetry lowering which removes the equivalence of two oxygen atoms causes a fundamental quantum mechanical question; is it possible to decide whether the core hole is localized on the right oxygen atom or on the left? Here we report the direct observation of the symmetry lowering of the CO₂ induced by O1s photoionization.

IX-W Study of Electronic Structure of Organic Thin Film and Organic/Inorganic Interface

Organic semiconductors have gained increasing interest because of their highly potential uses in various molecular devices. To clarify the electronic processes at the organic/inorganic interface, various characterization techniques such as high-resolution ultraviolet photoemission spectroscopy (UPS) and near-edge x-ray absorption fine structure (NEXAFS) have been performed for organic thin film systems, because the origin of the energy position and the bandwidth of UPS spectra are keys to understand the interface properties such as the energy level alignment at the interface, intermolecular or molecule-substrate interactions, and carrier transport process. Energy, vibronic coupling and lifetime of a hole created in the highest occupied molecular orbital (HOMO) state in the organic thin film play a crucial role in the hole transport through the film and the electron injection from an electrode to the ionized molecule. The HOMO band in UPS spectra in principle involves such information about the hole, and thus offers a variety of key information that is necessary to unravel fundamental mechanism in carrier transport properties in organic devices.

IX-W-1 Impact of an Interface Dipole Layer on Molecular Level Alignment at an Organic-Conductor Interface Studied by UPS

KERA, Satoshi; YABUCHI, Yousuke¹; YAMANE, Hiroyuki¹; SETOYAMA, Hiroyuki¹; OKUDAIRA, K. Koji¹; KAHN, Antoine²; UENO, Nobuo¹
(¹Chiba Univ.; ²Princeton Univ.)

[*Phys. Rev. B* **70**, 085304 (6 pages) (2004)]

The effect of an interface dipole layer on the energy level alignment at organic-conductor interfaces is studied on a copper phthalocyanine (CuPc) monolayer/electric dipole layer/graphite system *via* ultraviolet photoemission spectroscopy (UPS) and metastable atom electron spectroscopy (MAES). An oriented monolayer of the OTi-phthalocyanine molecule (OTiPc), which has an electric dipole moment, is grown on graphite to yield a well-defined dipole layer with the vacuum side negatively charged. The CuPc monolayer is sequentially deposited on the dipole layer kept at 123 K. This weakly interacting system made of a very thin organic layer on top of a very thin dipole layer is in thermodynamic equilibrium. The UPS data from the system grown with and without the interface dipole layer show that the binding energy of the highest occupied state of the CuPc monolayer decreases when the dipole layer is inserted. The binding energy shift is in excellent agreement with the increase in vacuum level energy of the graphite substrate upon deposition of the dipole layer. The results show that the Fermi level of the CuPc shifts toward the valence states when the interface dipole layer is inserted.

IX-W-2 HOMO-Band Fine Structure of OTi- and Pb-Phthalocyanine Ultrathin Films: Effects of the Electric Dipole Layer

YAMANE, Hiroyuki¹; HONDA, Hiroyuki¹; FUKAGAWA, Hirohiko¹; OHYAMA, Mitsuharu¹; HINUMA, Yoyo¹; KERA, Satoshi; OKUDAIRA, K. Koji¹; UENO, Nobuo¹
(¹Chiba Univ.)

[*J. Electron Spectrosc.* **137-140**, 223–227 (2004)]

Ultraviolet photoelectron spectra were measured for titanyl- and lead-phthalocyanine ultrathin films prepared on graphite in order to study effects of the electric dipole layer on the organic energy levels. Each of these molecules has an electric dipole perpendicular to the molecular plane, and hence a well-defined electric dipole layer could be intentionally prepared by using oriented monolayer of these molecules. For as-grown films the observed highest occupied molecular orbital (HOMO) band consists of many peaks that could be assigned to different molecular orientations/aggregations. For well-oriented monolayer films obtained by annealing the as-grown films, we observed a very sharp HOMO band with two satellites for both molecules as for copper phthalocyanine. Difference of binding energy of HOMO bands between the oriented monolayer and the doublelayer in which molecular dipoles are cancelled was found to agree with the vacuum level shift for both molecules, leading to important conclusions that (1) the molecular energy level with respect to the substrate Fermi level is changed when the molecule is in the dipole-layer and (2) the binding-energy shift corresponds with the vacuum level shift.

IX-W-3 Photoelectron Fine Structures of Uppermost Valence Band for Well-Characterized ClAl-Phthalocyanine Ultrathin Film: UPS and MAES Study

KERA, Satoshi; YAMANE, Hiroyuki¹; HONDA, Hiroyuki¹; FUKAGAWA, Hirohiko¹; OKUDAIRA, K. Koji¹; UENO, Nobuo¹
(¹Chiba Univ.)

[*Surf. Sci.* **566-568**, 571–578 (2004)]

Metastable atom electron spectroscopy was used to characterize monolayer formation of chloroaluminum phthalocyanine (ClAlPc) prepared on graphite. For as-grown film, molecules form island structure of staggered doublelayers on the substrate. By annealing the film, molecules diffuse to form a uniform monolayer where all the molecules are oriented flat with Cl atom directed to the vacuum. After the confirmation of the oriented monolayer formation, high-resolution ultraviolet photoelectron spectra were measured to study

effects of the molecular orientation on the energy levels. ClAlPc has an electric dipole perpendicular to the molecular plane, hence a well-defined electric dipole layer could be intentionally prepared by using the oriented monolayer. Difference of binding energies of HOMO bands between the oriented monolayer and the doublelayer was found to agree with the vacuum level shift, leading to a conclusion that the molecular energy level with respect to the substrate Fermi level is changed when the molecule is in the dipole-layer field.

IX-W-4 Study of Excited States of Fluorinated Copper Phthalocyanine by Inner Shell Excitation

OKUDAIRA, K. Koji¹; SETOYAMA, Hiroyuki¹;
YAGI, Hideki¹; MASE, Kazuhiko²; KERA, Satoshi;
KAHN, Antoine³; UENO, Nobuo¹
(¹Chiba Univ.; ²AIST; ³Princeton Univ.)

[*J. Electron Spectrosc.* **137-140**, 137–140 (2004)]

Near edge X-ray absorption fine structure (NEXAFS) spectra of hexadecafluoro copper phthalocyanine (FCuPc) films (thickness of 50 Å) on MoS₂ substrates were observed near the carbon (C) and fluorine (F) K-edges. From the analysis of the dependence of C and F K-edge NEXAFS spectra on the photon incidence angle (α), the average molecular tilt angle was determined to be 30°. The lowest and second lowest peaks in the F K-edge NEXAFS were assigned to the transition to σ^* . In the ion time-of-flight mass spectra of FCuPc excited by photons near the F K-edge, F⁺, CF⁺, and CF₃⁺ ions were mainly observed. These results indicate that C–C bonds as well as C–F bonds are broken by the photon irradiation. From the analysis of the partial ion yield spectra of F⁺ and CF⁺ near the F K-edge, the lowest and second lowest peaks in the F K-edge NEXAFS spectra could be assigned to transitions to $\sigma(\text{C–F})^*$ and $\sigma(\text{C–C})^*$, respectively.

IX-W-5 Simulation Study of Angle-Resolved Photoemission Spectra and Intramolecular Energy-Band Dispersion of a PTFE Oligomer Film

YOSHIMURA, Daisuke¹; ISHII, Hisao²; OUCHI, Yukio³; MIYAMAE, Takayuki⁴; HASEGAWA, Shinji⁵; OKUDAIRA, K. Koji⁶; UENO, Nobuo⁶; SEKI, Kazuhiko³
(¹IMS and Nagoya Univ.; ²Tohoku Univ.; ³Nagoya Univ.; ⁴AIST; ⁵Fuji Xerox; ⁶Chiba Univ.)

[*J. Chem. Phys.* **120**, 10753–10762 (2004)]

Theoretical simulations of the angle-resolved ultraviolet photoemission spectra for the oligomer of poly(tetrafluoroethylene) ((CF₂)_n; PTFE) was performed using the independent-atomic-center (IAC) approximation combined with *ab initio* molecular orbital (MO) calculations. Previously observed normal-emission spectra for the end-on oriented sample (with long-chain axis being perpendicular to the surface) showed the incident photon-energy ($h\nu$) dependence due to the

intramolecular energy-band dispersion along the one-dimensional chain,¹⁾ and the present simulations successfully reproduced this $h\nu$ -dependence of the observed spectra. We employed the experimentally observed helical structure for PTFE oligomers for the simulations. We also calculated the density of states (DOS) for the planar zigzag structure, and examined the changes in the electronic structure due to the difference in the molecular structure by comparing the DOS for the helical and planar zigzag structures. Only little change in the DOS was found between these structures, showing little change of the electronic structure between these conformations. We also evaluated the inner-potential V_0 , which is the parameter defining the energy origin of the free-electron-like final state, and checked the validity of the value of –10 eV estimated in our previous study using the experimentally observed $h\nu$ -dependence of the peak intensity.¹⁾ The estimation of V_0 was performed by pursuing the best agreement between the energy-band dispersion ($E = E(\mathbf{k})$) relation along the chain direction obtained from the simulated spectra and the experimentally deduced one. An excellent agreement in the topmost band was achieved when the assumed inner potential V_0 was set about zero. This value of V_0 is much different from the value of $V_0 = -10$ eV in the previous study, suggesting the invalidity of the previous assumption at the estimation of V_0 from the peak intensity variation with $h\nu$. Using the presently obtained V_0 , we could derive more reliable $E = E(\mathbf{k})$ dispersion relation from the observed ARUPS spectra. The comparison of this newly derived relation gave good agreement with theoretically calculated $E = E(\mathbf{k})$ relations, in contrast to the poor agreement for the previous results with $V_0 = -10$ eV.

Reference

- 1) T. Miyamae, S. Hasegawa, D. Yoshimura, H. Ishii, N. Ueno and K. Seki, *J. Chem. Phys.* **112**, 3333–3338 (2000).

IX-X Effects of High Magnetic Field on Chemical and Physical Processes

We have studied the effects of high magnetic field on chemical reaction and physical processes of diamagnetic and paramagnetic materials to unravel the mechanisms of the interaction of matter and magnetic field and to develop unique methods controlling chemical and physical processes and improving chemical and physical properties of functional materials. Currently we are using a vertical superconducting magnet which can generate high magnetic fields (15 T, $1500 \text{ T}^2/\text{m}$) in a $40 \text{ }\phi$ bore tube. Last year, we have succeeded, for the first time, to induce 3-dimensional morphological chirality in zinc silicate membrane tube using a high magnetic field. This year, from *in situ* observation, we have verified the mechanism. The Lorentz force on ions induces remarkable convection of a solution in silicate garden reaction. Some other interesting effects of magnetic fields were also studied.

IX-X-1 3-Dimensional Morphological Chirality Induction in Silicate Garden Reaction Using a Magnetic Field

DUAN, Wenyong¹; UECHI, Ichiro¹; KITAMURA, Shu²; FUJIWARA, Yoshihisa²; TANIMOTO, Yoshifumi¹

(¹IMS and Hiroshima Univ.; ²Hiroshima Univ.)

We have reported that *three-dimensional morphological chirality* can be induced in silicate membrane tubes formed from the reaction of sodium silicate aqueous solution and zinc sulfate crystals by using vertical magnetic fields (5–15 T).¹⁾ In magnetic fields right-handed helical tubes grow along the inner surface of the vessel wall, whereas left-handed tubes grow along the outer surface of the glass rod placed in the vessel. In order to examine whether this new effect is generally observed in silicate garden reaction, we have studied many silicate garden reactions using different metal salt crystals. Morphological chirality is induced in membrane tubes prepared from magnesium chloride, copper sulfate, manganese sulfate, and iron sulfate crystals, indicating that this effect is common in silicate garden reaction. Paramagnetism of metal ion such as copper ion is unimportant for chirality induction, indicating that magnetic force cannot induce morphological chirality. Furthermore, in magnetic fields membrane tubes grown apart from the vessel wall are twisted to the opposite direction to those grown along the inner surface of the wall, as shown in Figure 1.

In order to verify the mechanism, *in situ* observation of the reaction using magnesium salt crystals was carried out in a bore tube of a magnet. At zero field, no convection of sodium silicate aqueous solution was observed regardless of magnesium chloride crystals. In the presence of 15 T vigorous convection was observed only when the crystals were added to the solution. It was shown that helical tubes near the vessel wall grow along the convection, whereas tubes apart the wall are twisted by the convection. It is now verified that Lorentz force on ions blowing out from the membrane tubes induces remarkable convection of the bulk solution.

Reference

- 1) I. Uechi, A. Katsuki, L. Dunin-Barkovskiy and Y. Tanimoto, *J. Phys. Chem. B* **108**, 2527–2530 (2004).

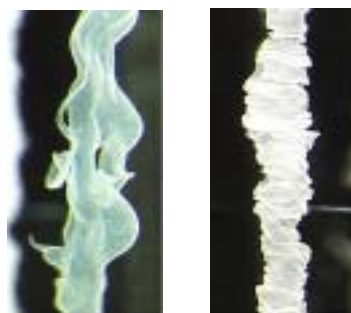


Figure 1. Photos of zinc silicate membrane tubes grown apart from a vessel wall at zero field (left) and 12 T (right). (Magnification; 175)

IX-X-2 *In Situ* Observation of the Effects of a High Magnetic Field on the Growth of Silver Dendrites

KATSUKI, Akio¹; TANIMOTO, Yoshifumi

(¹Shinshu Univ.)

We have showed 3-dimensional morphology and chemical yields of silver dendrites generated by the liquid/solid redox reaction between silver ion and copper metal were remarkably affected by *vertical* high magnetic fields.¹⁾ In order to clarify the mechanisms, we have undertaken *in situ* observation of the silver dendrite formation reaction in 2-dimensional system. A thin plate of zinc metal ($0.1 \text{ mm} \times 20 \text{ mm} \times 5 \text{ mm}$) was sandwiched with two plastic plates ($2 \text{ mm} \times 20 \text{ mm} \times 55 \text{ mm}$), and silver nitrate aqueous solution was added to the space between two plates. At zero field, dendrites on the upper side of the metal plate grew steadily and no convection of the solution was observed. At 15 T, the top of dendrites underwent precession with bottom fixed. This unique phenomenon indicates that the solution near the dendrites undergoes convection due to the Lorentz force on the flow of ions. Because of concentration gradient of silver ions near the reactive zone of dendrites, silver ions move to dendrite surface and Lorentz force affects the flow of silver ions, leading to the convection of the solution near dendrites. Since dendrites are composed of many small crystals, they are not rigid but flexible. Circular convection of the solution near the dendrites induces precession of the flexible dendrites. This means that Lorentz force is very important for the reaction where concentration gradient of ions is induced during the reaction.

Reference

1) A. Katsuki, I. Uechi and Y. Tanimoto, *Bull. Chem. Soc. Jpn.* **77**, 275–279 (2004).

IX-X-3 Formation of Protein Crystals (Orthorhombic Lysozyme) in a Pseudo-Microgravity Environment Obtained by a Superconducting Magnet

YIN, D. C.¹; WAKAYAMA, N. I.²; HARATA, K.³; FUJIWARA, Masao; KIYOSHI, T.²; WADA, H.²; HUANG, W. D.⁴; TANIMOTO, Yoshifumi
(¹NIMS and Northwestern Polytechnical Univ., China; ²NIMS; ³AIST; ⁴Northwestern Polytechnical Univ., China)

[*J. Cryst. Growth* **270**, 184–191 (2004)]

As one of the best candidates for simulating the microgravity conditions in space, low gravity environments provided by applying an upward magnetic force has been considered to grow protein crystals. Since 2002, the stable and long-time durable microgravity generated by a superconducting magnet has been available for protein crystal growth. In this paper, for the first time, we grew protein crystals (orthorhombic lysozyme crystals) at pseudo-microgravity. The present study showed that pseudo-microgravity improves the crystal quality effectively and reproducibly. The application of strong magnetic field also improves the crystal quality. Further verification of the combined effects of microgravity and magnetic field itself may lead to a more general means to grow high quality protein crystals.

IX-X-4 Magnetic Field Effects upon Macroscopic Plastic Deformation of Diamagnetic Single Crystals Containing Paramagnetic Impurity

DUNIN-BARKOVSKIY, L. R.; MORGUNOV, R. B.¹; TANIMOTO, Yoshifumi
(¹IMS and ISSIP, Chernogolovka)

It is known that macroscopic magnetoplastic effects in inorganic crystals containing paramagnetic impurity are mainly caused by spin-dependent solid reactions in the system of crystal structure defects. In spite of wide interest to the topic, there is so long a lack of understanding of the mechanisms of such effects. In this work we studied magnetic field effects on plastic deformation of NaCl:Eu single crystals. The crystals were annealed at 770 K and quenched to room temperature. Then they were deformed at room temperature in the absence and presence of a magnetic field (15 T). The field affects the shape of stress-strain diagram, in particular decreases the yield stress by approximately 100%, as shown in Figure 1. Besides, partial or complete suppression of the drop deformation (*i.e.*, Portevin-Le Chaterlier effect), caused by dynamic interaction between movable dislocations and atoms of dissolved impurity, was observed for the first time.

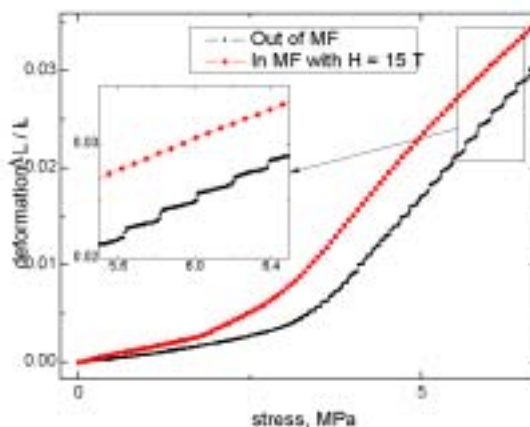


Figure 1. Magnetic field effects on stress-strain diagram of NaCl:Eu single crystal.

IX-X-5 Effect of Horizontal High Magnetic Field on the Movement of *E. coli*

TANIMOTO, Yoshifumi¹; OGAWA, Seiji²; FUJITANI, Kiyomi²; FUJIWARA, Yoshihisa²; IZUMI, Shunsuke²; HIRATA, Toshifumi²
(¹IMS and Hiroshima Univ.; ²Hiroshima Univ.)

[*Environ. Sci.* in press]

Effects of a high magnetic field gradient (8 T, *ca.* 400 T²/m, horizontal) on the behavior of *E. coli* were examined. An *E. coli* suspended solution was injected in one end of a glass tube (5 mmφ × 150 mm) filled with viscous medium containing sodium nitrate. They move along the tube axis because of chemotaxis to nitrate ion. The speeds for movement from a high (8 T) to a low field (1.5 T) and for the opposite movement are 1.35 and 0.49 cm/h, respectively; it is 0.65 cm/h at a zero field. It is found that the magnetic force hastens the downfield movement of *diamagnetic E. coli* and impedes the up-field movement.

IX-Y Theoretical and Computational Study on Gas Phase Reactions

1. Quantum chemical calculations are used to produce potential energy surface (PES) to do reaction dynamics simulations. We develop the methodology to generate PES efficiently and automatically using quantum chemical calculation results. The method does not need any derivative information in quantum chemical calculations.
2. We search a reasonable pathway to form H₂ and the other interstellar molecules *via* PAH related catalysts.
3. We also calculate (electronic) CD spectra to determine the absolute configuration of several chiral molecules in collaboration with experimentalists.

IX-Y-1 Aromatic Character of Annelated Dimethyldihydropyrenes

AIHARA, Jun-ichi¹; ISHIDA, Toshimasa
(¹Shizuoka Univ.)

[*J. Phys. Org. Chem.* **17**, 393–398(2004)]

Aromaticity is one of the fascinating concepts in modern organic chemistry. It has been defined in structural, magnetic and energetic terms. Historically, many chemists have discussed aromaticity most conveniently in terms of ¹H chemical shifts. Mitchell and co-workers noted that ¹H chemical shifts of the internal methyl groups in dimethyldihydropyrene (DDP) and its annelated derivatives serve to assess the relative local aromaticities of the DDP nuclei. They recently estimated the order of aromaticity for DDP nuclei in annelated derivatives using nucleus-independent chemical shifts (NICS). We found that two graphtheoretically defined energetic quantities, percentage topological resonance energy (% TRE) and bond resonance energy (BRE), can be used to predict readily the relative aromaticities of these hydrocarbons and their DDP nuclei, respectively. Since these quantities are not dependent on the areas of individual rings, they are better suited for estimating the degree of aromaticity.

IX-Y-2 Possible Molecular Hydrogen Formation Mediated by the Inner and Outer Carbon Atoms of Typical PAH Cations

HIRAMA, Mutsumi¹; ISHIDA, Toshimasa;
AIHARA, Jun-ichi¹
(¹Shizuoka Univ.)

[*Chem. Phys.* **305**, 307–316 (2004)]

We have been exploring the possibility of H₂ formation mediated by the radical cations of gaseous polycyclic aromatic hydrocarbons (PAHs). In this study, we estimated the catalytic ability of the inner carbon atoms of some typical PAH cations at the B3LYP/6-31G** level of theory and compared it with that of the outer carbon atoms. We presumed as before that H₂ is formed by way of two elementary reactions, the addition of an H atom to a PAH cation and the H abstraction from the resulting arenium ion by another H atom to yield H₂. We found that both reactions proceed without any activation energy. It follows that almost all carbon atoms of a PAH cation give sites for molecular hydro-

gen formation. Since there are large compact PAHs abundantly in space, the H₂ formation at the inner carbon atoms of such PAH cations can never be overlooked. Even if inner carbon atoms might be less reactive than peripheral ones, there are many inner carbon atoms in large compact PAH cations.

IX-Y-3 One-Pot Synthesis of Helical Aromatics: Stereoselectivity, Stability against Racemization, and Assignment of Absolute Configuration Assisted by Experimental and Theoretical Circular Dichroism

WATANABE, Masashi¹; SUZUKI, Hiroshi¹;
TANAKA, Yasutaka; ISHIDA, Toshimasa;
OSHIKAWA, Tatsuo²; TORII, Akiyoshi³
(¹Shizuoka Univ.; ²Numazu College Tech.; ³Saga Univ.)

[*J. Org. Chem.* in press]

Helical aromatics (**1**) were synthesized *via* one step in good quantity by solvent-free condensation of *N,N'*-*p*-phenylenediamine (**2**) and various carboxylic acids in the presence of Lewis acid. Microwave irradiation greatly facilitated the condensation reaction to furnish **1** with a 100% diastereo- and a 50% enantioselectivity, when a chiral carboxylic acid was utilized. **1f**, derived from 2-methylglutaric acid, was quite stable, no racemization taking place even at 200 °C. The assignment of the absolute configurations to the helical aromatics has been attempted by CD exciton chirality method and comparison of experimental and theoretical CD spectra calculated by time-dependent density functional theory.

IX-Y-4 A Local Interpolation Scheme Using No Derivatives in Potential Sampling: Application to OH + H₂ System

ISHIDA, Toshimasa; SCHATZ, George C.¹
(¹Northwestern Univ.)

[in preparation]

We recently proposed a local interpolation scheme, in which interpolant moving least squares (IMLS) and the modified Shepard interpolation proposed by Collins are employed to describe potential energy surfaces. This IMLS/Shepard scheme is applicable to do potential interpolation with quantum chemical results for which analytical derivatives are not available. We applied the scheme to a four atomic system OH + H₂ → H₂O + H

reaction. As for the former system, we compared the results with those based on the modified Shepard interpolation using second order Taylor expansions. An analytical surface is used to define the potential function so that errors in the interpolation function may accurately be determined. We found that the energy and gradient errors in the present scheme is comparable to those in the modified Shepard scheme. Note that the present scheme does not utilize derivative and hessian information whereas the Shepard interpolation does. The accuracy in the IMLS/Shepard scheme is surprising, but can be explained by the more global nature of the interpolation.

IX-Y-5 Possible Interstellar Molecule Formations Mediated by Naphthalene Cation

HIRAMA, Mutsumi¹; ISHIDA, Toshimasa;
AIHARA, Jun-ichi¹
(¹Shizuoka Univ.)

[in preparation]

We have studied the possibilities of interstellar molecule formation mediated by the radical cations in the gas phase. In this letter, we explored the catalytic role of a typical PAH cation, a naphthalene cation, at the both B3LYP/6-31G** and MP2/6-31G** levels of theory. We presumed that interstellar molecule is formed by way of two elementary reactions: the addition of an H atom to a PAH cation and the H abstraction from the resulting arenium ion by one interstellar molecular species to form another interstellar molecular species. It was found that the first reactions proceed with no activation energies. Refinement of the activation energies with both spin-projected and unrestricted MP2 procedures confirmed no or very small activation energies for the second reactions.

We employ the simplest PAH, a naphthalene, as molecular catalyst and consider that the naphthalenium ion is one of the key intermediates not only in the formation of molecular hydrogen but also in the formation of interstellar molecular species. We studied some formations of their species, *i.e.*, HCCH, CH₄, HCN, HNC, H₂O, NH₃, NH₂, CH₃, and CH₂. All of these species and these precursors have observed in space.

IX-Y-6 Molecular Rattles Using Excited States and Non-Adiabatic Transition

ISHIDA, Toshimasa; NANBU, Shinkoh;
NAKAMURA, Hiroki

[in preparation]

Non-adiabatic phenomena play crucial roles in the molecular science, in particular, in the molecular material field. Nakamura and Nanbu proposed the idea for the molecular switching with aggressive use of the phenomena although the virtual system composed of an ideal one-dimensional finite periodic potential system was used. The key-phenomena in the idea are the complete reflection and complete transmission. Once we find the appropriate condition for those phenomena in

the corresponding system, the molecular motion can be completely controlled without any exception.

We newly propose the application of our idea to the transmission of hydrogen atom through cyclic molecule. This may be regarded as a model of encapsulation by carbon nanotubes.

We explored lots of systems with theoretical calculations, and finally it is found that several model systems seem to be suitable. Two of them are (1) cyclopentadienyl radical (C₅H₅) + H reaction model and (2) C₉H₉ + alkaline atom system.

In these systems, we found complete transmission and reflection, which is based on two non-adiabatic transition of non-adiabatic tunneling type. We will discuss possible application to real systems.

IX-Y-7 Quantum Chemical Study of H₂ Formation Reaction *via* the Benzene Cation Catalyst

HIRAMA, Mutsumi¹; AIHARA, Jun-ichi¹; ISHIDA, Toshimasa
(¹Shizuoka Univ.)

[in preparation]

We have been exploring a possibility that polycyclic aromatic hydrocarbon (PAH) cations may catalyze the H₂ formation because PAHs are ubiquitous in interstellar space and are probably partly ionized by stellar UV radiation. Benzene is not a PAH, but is an aromatic hydrocarbon, so that it is expected to give similar energy profile to PAHs. Thus, we undertake to use benzene cations to investigate the effect of more sophisticated method for electron correlation on the energy profile of the H₂ formation reaction.

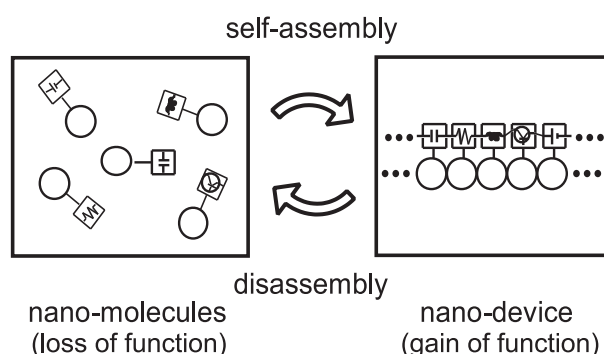


We employed coupled cluster singles and doubles (CCSD) and its modification with the third order perturbation energy (CCSD(T)) as well as QCISD(T) at the MP2-optimized geometries to make comparison of the results with the B3LYP and MP2 ones to estimate higher correlation effects. In addition, use of both the B3LYP and MP2 results proposed by Turecek was evaluated. CCSD, CCSD(T), and QCISD(T) calculations gave us activation energies between B3LYP and MP2 values. From these results, hybrid use of B3LYP and MP2 would be justified to estimate activation energies for larger PAH cation catalyst systems.

IX-Z Macromolecular Self-Assembly Opens the Way for Development of Novel Materials That Have Characteristics of Cellular Systems

Methods to integrate functional molecules into well-defined nano structures is a key for fabrication of future materials. Nano-integrated circuits may be afforded by elaborate arrangements of various molecular- and nano-devices. Self-assembly is a strong tool for integration of molecules into various nano structures. Self-assembly, however, tends to give polymorphism and structural defects in the assembled structures. Furthermore, functions of elaborate molecular systems should be sensitive to small structural damages and heat dissipation. For development of the future materials, thus, one should employ a self-assembly process that selectively affords a single, well-defined supramolecular structure to suppress polymorphism. It is also necessary that the formed device is repairable to be robust to damages and defects. We examine such a design strategy that has not yet been examined to date (Figure 1; see also Special Research Project (c)).

Figure 1. A concept of the nano-device that functions on-demand. The device does not function until on-demand self-assembly of nano functional blocks, and can easily be decomposed into the reusable components on demand.



IX-Z-1 Fabrication of Nano-Devices on the Principle of Cellular Supramolecular System

OBA, Toru; HANASAKI, Mitsuru¹; SATO, Michihiro¹; MINABE, Masahiro¹
(¹Utsunomiya Univ.)

[*Photosynthesis: Fundamental Aspects to Global Perspectives in press*]

Development of molecular devices has attracted much attention in the field of electronics and photo-electronics. For global, sustainable development, molecular devices and nano-devices should be reusable, repairable, and bio-degradable, which has not been considered to date. We thus aimed at development of an artificial photosynthetic device as a prototype of the flexible (supra)molecular system that functioned on demand (Figure 1). We employed naturally occurring nano-tube, 'microtubule' (MT), to integrate functional molecules into a nano ordered structure. We prepared tubulins (Tubs), component proteins of MT, conjugated with a fluorophore for light-harvesting and with a photosensitizer-labeled hemoprotein for charge separation, respectively, and mixed them simply. Each time these functional blocks self-assembled to form MTs in the assembly/disassembly cycle, solar energy absorbed by the antenna fluorophore migrated to the sensitizer, leading to charge separation between the sensitizer and the heme. The nano-device can easily be decomposed into the components on demand, and the components can readily reassemble on demand to recover the function again.

IX-Z-2 Synthesis and Properties of Novel Cationic Chlorophyll Derivatives

OBA, Toru; TAKATOYA, Haruki¹; TOBITA, Hiromi¹; UGAJIN, Aya¹; OGURA, Koji¹; MINABE, Masahiro¹
(¹Utsunomiya Univ.)

[*Photosynthesis: Fundamental Aspects to Global Perspectives in press*]

Not only metal nano particles but also biomolecules such as DNA, phospholipids, proteins and their supra-molecules have been studied for development of molecular devices. It is of much interest to conjugate chlorophylls (Chls), quite abundant photofunctional molecules in nature, with these biomolecules in water for fabrication of novel photofunctional materials such as artificial photosynthetic devices. Chl derivatives that carry cationic charges may be advantageous for interaction with anionic surfaces of the biomolecules and their supra-molecules. The conjugation is, however, quite difficult, because, in general, Chls are insoluble in water, resulting in facile formation of higher aggregates. We prepared Chl derivatives that had cationic polymer moiety. Condensation of cationic polymer improved water-solubility, lowered the aggregation number, and enabled conjugation with proteins. The cationic, water-soluble Chl derivative is thus a useful tool for various investigations and applications.

IX-Z-3 Physicochemical Studies on the Molecular Mechanism of Photosynthesis

OBA, Toru; TAMIAKI, Hitoshi¹
 (¹Ritsumeikan Univ.)

[*Photosynthesis: Fundamental Aspects to Global Perspectives* in press]

Since chlorophylls (Chls) and bacteriochlorophylls (BChls) are highly asymmetric molecules, an external ligand can coordinate to the central Mg atom of (B)Chls from either of the two sides of the chlorin macrocycle. We found that the 'back' side (Figure 1) is favored for the ligand coordination, by survey of the highly resolved crystal structures of photosynthetic proteins and by theoretical calculations of model molecules. We have recently found that the 'back' type complex is also the major isomer in two newly resolved photosynthetic proteins. In light-harvesting complex II, 6 of 8 Chl *a* and 4 of 6 Chl *b* are the 'back'-type complexes, respectively. Among 28 ligand-identified Chls in the photosystem 2 core complex, 22 are the 'back' stereoisomers. Further calculations on the virtual chlorin molecules revealed the origin of the energy gap between the 'back' and the 'face' stereoisomers. We also discuss yet undetermined nomenclatures for the macrocycle faces of (B)Chls.

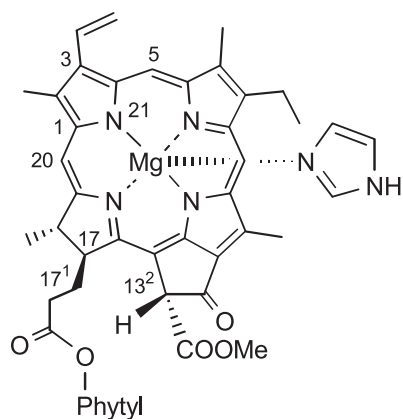


Figure 1. Molecular structure of the 'back' type chlorophyll *a*-imidazole complex.